University of Natural Resources and Life Science Vienna
Christian Doppler Laboratory on Biotechnology of Skin Aging
(Assoc. Prof. Dr. Johannes Grillari)

The role of the protein SNEV$^{hPrp19/hPso4}$ in function and morphology of human dermal fibroblasts and human epidermal keratinocytes

Master thesis

University of Veterinary Medicine Vienna

submitted by
Lisa Kleissl, BSc

submitted at
Institut für Physiologie, Pathophysiologie und Biophysik
Veterinärmedizinische Universität Wien

Vienna, June 2017

Supervision

Internal Supervision: Univ.-Prof. Dr.med. Dr.med.vet. Reinhold Erben

External Supervision: Assoc. Prof. Dr. Johannes Grillari

Statutory Declaration

“I declare in lieu of an oath that I have written this master thesis myself and that I have not used any sources or resources other than stated for its preparation. I further declare that I have clearly indicated all direct and indirect quotations. This master thesis has not been submitted elsewhere for examination purposes.”

Date: **Signature**

Abstract

SNEV$^{hPrp19/hPso4}$ is a multifunctional protein involved in several crucial cellular pathways such as mRNA splicing, DNA repair, ubiquitin/proteasome associated protein degradation, neuronal differentiation and life span regulation. It's already known that *SNEV*$^{hPrp19/hPso4}$ overexpression extends the life span of human umbilical vain endothelial cells (HUVECs), however, its molecular function is not fully understood yet. Considering all these facts it seems obvious that this protein plays an important role in the aging process. Since the human skin provides one of the most visual aging transformations, and premature skin aging as a consequence of oxidative stress and DNA damage is a frequently seen effect, it would be interesting to asses if the overexpression of the DNA repair factor *SNEV*$^{hPrp19/hPso4}$ could improve DNA repair and increase the life or health span in cells of the human skin. The aim of this study was to generate a stable *SNEV*$^{hPrp19/hPso4}$ overexpressing human dermal fibroblast cell line and to characterize this cell line with respect to growth behaviour, morphology, cellular senescence and wound healing. Surprisingly, in contrast to previous results obtained in endothelial cells, *SNEV*$^{hPrp19/hPso4}$ overexpression led to a reduced lifespan in human fibroblasts. However, we found that *SNEV*$^{hPrp19/hPso4}$ overexpression changed the fibroblast morphology towards a more papillary/juvenile phenotype, compared to empty vector control cells. To get more insights into the role of *SNEV*$^{hPrp19/hPso4}$ in skin function, wound healing assays, collagen contraction assays as well as the overexpression of *SNEV*$^{hPrp19/hPso4}$ in keratinocytes were performed. We discovered that SNEV$^{hPrp19/hPso4}$ overexpressing fibroblasts enhance keratinocyte migration to the wounded area, suggesting that it has a positive effect on wound healing. We also generated stable *SNEV*$^{hPrp19/hPso4}$ overexpressing keratinocyte cell lines, but in contrast to fibroblasts, we observed neither effects on growth, nor on cellular morphology. In summary, we found that *SNEV*$^{hPrp19/hPso4}$ modulates dermal fibroblast morphology, growth and communication with epidermal keratinocytes. The precise mechanisms remain subject to future studies.

Keywords: skin aging, *SNEV*$^{hPrp19/hPso4}$, papillary to reticular transition, DNA damage, DNA repair, wound healing

Kurzfassung

SNEV$^{hPrp19/hPso4}$ ist ein multifunktionelles Protein, welches in vielen verschiedenen zellulären Mechanismen wie zum Beispiel mRNA Splicing, DNA Reparatur, Proteinabbau, neuronale Differenzierung, sowie in der Regulation der zellulären Lebensspanne von entscheidender Bedeutung ist. Die replikative Lebensdauer von humanen Endothelzellen (HUVECs) wird durch die Überexpression dieses Proteins deutlich verlängert. Der genaue, zugrundeliegende molekularbiologische Mechanismus ist jedoch noch nicht völlig klar. Die menschliche Haut unterliegt während des Alterns einem sichtbar starken Veränderungsprozess und verschiedenste Arten von Stress, zum Beispiel auf Grund von DNA-schädigender UV-Strahlung, führen zu einer frühzeitigen Hautalterung. Ziel dieser Diplomarbeit war es herauszufinden, ob eine Überexpression dieses DNA Reparatur-Faktors zu einer Verlängerung der Lebensspanne bzw. zu längerer Gesundheit in Hautzellen führt. Zu diesem Zweck haben wir *SNEV*$^{hPrp19/hPso4}$ stabil in humanen dermalen Fibroblasten überexprimiert und die daraus resultierenden Auswirkungen untersucht. Im Gengensatz zu früheren Beobachtungen in Endothelzellen bewirkte eine *SNEV*$^{hPrp19/hPso4}$ Überexpression in Fibroblasten eine Reduktion der zellulären Lebensspanne. Jedoch gelang es mittels Immunfluoreszenz die Morphologie von *SNEV*$^{hPrp19/hPso4}$ überexprimierenden Fibroblasten, im Vergleich zu der Kontrollzellline, als papillärer/juveniler zu charakterisieren. Um einen tieferen Einblick in die Rolle von *SNEV*$^{hPrp19/hPso4}$ in der Hautfunktion zu bekommen, wurden Wundheilungs Assays, Collagen Contraction Assays und die Überexpression in Keratinozyten durchgeführt. Wir fanden heraus, dass *SNEV*$^{hPrp19/hPso4}$ überexprimierende Fibroblasten die Migration von Keratinozyten in verwundetes Areal fördern und *SNEV*$^{hPrp19/hPso4}$ somit einen vermutlich positiven Effekt auf die Wundheilung hat. Zudem konnten stabile *SNEV*$^{hPrp19/hPso4}$ überexprimierende Keratinozyten-Zelllinien erzeugt werden. Allerdings konnte in Keratinozyten im Hinblick auf Wachstum und Morphologie kein deutlicher Effekt beobachtet werden. In Summe konnten wir zeigen, dass *SNEV*$^{hPrp19/hPso4}$ in dermalen Fibroblasten eine wichtige Rolle bezüglich Wachstum, Morphologie, Kommunikation mit epidermalen Keratinozyten und somit für die Hautgesundheit spielt. Die zugrundeliegenden molekularen Mechanismen erfordern weitere, intensive Nachforschungen.

Acknowledgments

First of all I want to display my gratitude to Assoc. Prof. Dr. Johannes Grillari, who gave me the opportunity to write my master thesis and perform the necessary laboratory work in his research group, Grillari Labs at the University of Natural Resources and Life Science, Vienna. Thank you Giovanni for not being just my official supervisor but also a great mentor, who always had helpful advice. I also want to thank Univ.-Prof. Dr.med.vet. Reinhold Erben, who agreed to be my internal supervisor at the Veterinary University, Vienna.

At the same time I wish to thank Hanna Dellago with all of my heart. Thank you Hanna first, for giving me the opportunity to work with you on the “SNEV Project” and secondly, for not only supporting me in any scientific related questions and affairs, but also for being a good friend and mental succour. I learned a lot from you and really appreciate that I had the opportunity to work together with you.

Furthermore I also want to display my gratitude to all members of the research group Grillari Labs – Ingo, Markus, Regina and Lucy – who accepted me with any constraints and taught me a lot. Thank you also to all the other colleagues who I consider as good friends, from fellow students to post-docs. I enjoyed working with you in the lab as well as chatting at our “lunch breaks”. Last but not least I want to thank my family and friends for their support and nice words, also in harder times. Thanks Mama & Papa for giving me the opportunity to live the life I did so far. And thank you Chrisi!

Without any of them, this thesis wouldn’t have been possible.

Table of content

List of figures

List of tables

Abbreviations

ATM	Ataxia telangiectasia
ATP	Adenosine triphosphate
ATR	Ataxia telangiectasia mutated and Rad3 related
ATRIP	ATR interaction protein
α-SMA	α-smooth muscle actin
Cdc5L	Cell division cycle 5 protein
cDNA	Complementary DNA
Chk1	Checkpoint kinase 1
CNN	Caponin
DAPI	4′,6-Diamidin-2-phenylindol
DSB	Double strand break
ds-DNA	Double stranded DNA
DMEM	Dulbecco’s Modified Eagles Medium
DMSO	Dimethyl sulfoxide
DR	Diatry restriction
DDR	DNA damage response
ECM	Extracellular matrix
FCS	Fetal calf serum
GAPDH	Glyceraldehyde-3-phosphat dehydrogenase
GM-CSF	Granulocyte-macrophage colony stimulating factor
G418	Geneticin 418
HDF	Human diploid fibroblasts
HGPS	Hutchinson-Gilford Progeria Syndrome
hTERT	Human telomerase reverse transcriptase

HUVECs	Human umbilical vein endothelial cells
H2O2	Hydrogen peroxidase
ICL	Interstrand crosslinks
IGF	Insulin-like growth factor
IIS	Insulin and insulin-like growth factor signalling pathway
INK4/ART	Cycline-dependent kinase4/alternative reading frame
KGF	Keratinocyte growth factor
KGM-2	Keratinocyte growth media
MMP	Matrix metalloproteinase
MRN	Mre11-Rad50-Nb1
mRNA	Messenger ribonucleic acid
NFW	Nuclease free water
NHEJ	Non-homologous end joining
NHEK	Normal human epidermal keratinocytes
PBS	Phosphate buffered saline
PCNA	Proliferating cell nuclear antigen
PDPN	Podoplanin
PI3KI	Phosphatidylinositol 3-kinase
PRT	Papillary to reticular transition
qPCR	Real-time quantitative polymerase chain reaction
RPA	Replication protein A
ROS	Reactive oxygen species
RT-qPCR	Real time – quantitative polymerase chain reaction
SA-β-gal	Senescence associated β-galactosidase assay
SASP	Senescent-associated secretory phenotype
snRNPs	Small nuclear ribonucleoprotein

SSB	Single strand break
SNEV	Senescence evasion factor
ss-DNA	Single stranded DNA
TCR	Transcription coupled repair
TGM	Transglutaminase
TIMP	Tissue inhibitor of metalloproteinase
TREX	Transcription Export
UV	Ultraviolet radiation
WS	Werner Syndrome
XAB2	XPA-binding protein
XPA	Xeroderma pigmentosa group A protein

1 Introduction

1.1 Biology of Aging

Aging can be defined as a progressive general impairment of function, connected with an increased risk of death. Loss of function is usually associated with a higher susceptibility to diseases including Alzheimer, Rheumatoid Arthritis as well as cancer(Campisi 2013).

In evolution, aging is often attributed to a phenomenon termed antagonistic pleiotropy. This means that genes, which are beneficial in early-life survival but at the same time impair late-life viability are not eliminated by natural selection because they became active and, often they have already been passed on to the next generation. These genes accumulate and lead to a seemingly programmed aging(Williams 1957).

1.1.1 The hallmarks of aging

There are nine cellular and molecular hallmarks of aging as illustrated in Figure 1, which together determine the aging phenotype. All of them need to fulfil certain criteria: (I) manifestation during normal aging; (II) experimental aggravation of such a hallmark should result in an accelerated aging process; (III) on the other hand, experimental amelioration should retard the aging process and therefore increase viability(López-Otín et al. 2013).

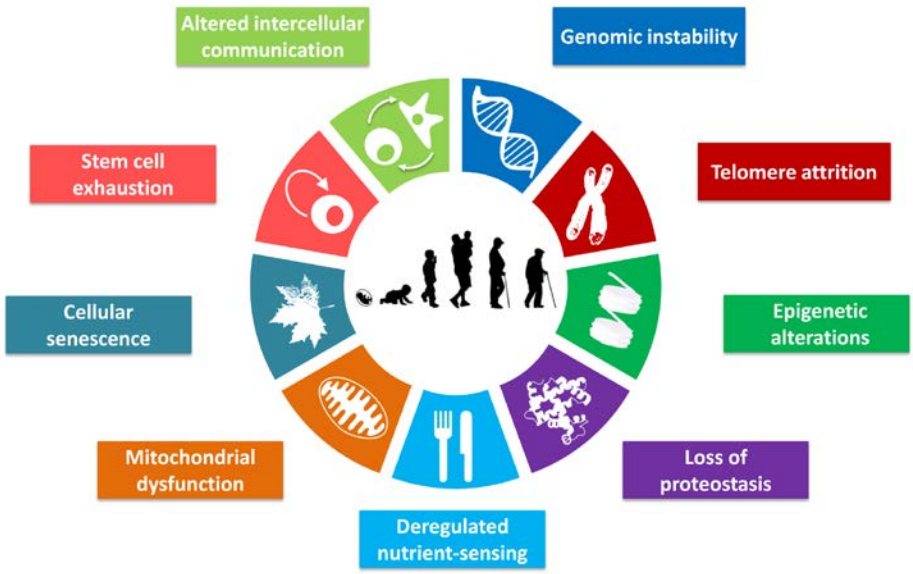

Figure 1: The nine hallmarks of aging. .Adopted from López-Otín et al. (2013)

The hallmarks of aging are:

Genomic instability

Genomic instability is a result of DNA damage caused by extrinsic and intrinsic DNA damaging agents as well as laminopathies, which are defined as defects in the nuclear architecture(Hoeijmakers 2009, Worman 2012). To counteract these processes, DNA repair pathways were evolved to maintain integrity and stability of the DNA. A dysfunction of such pathways therefore can lead to progeroid syndromes such as the Werner syndrome.(Lee et al. 2005a).

Telomere attrition

A phenomenon termed replicative senescence is the result of telomere exhaustion. The only enzyme capable of completely replicating the terminal ends of linear DNA is telomerase. This specialized DNA polymerase is usually not expressed in most mammalian somatic cells, hence at some time proliferation capacity is exhausted(HAYFLICK and MOORHEAD 1961). In telomerase-deficient mice premature aging could be reverted by genetically reactivating

telomerase(Jaskelioff et al. 2011). Increased telomerase activity allows cells to delay growth arrest and can lead to uncontrolled cell proliferation, enhancing the risk of cancer(Shay et al. 2001). Therefore, a finely tuned and balanced telomerase activity is important.

Epigenetic alterations

Epigenetic alterations are inheritable changes in the expression or function of a gene without a change in the DNA sequence(Jones and Baylin 2002). Fraga and Esteller defined some well-known age associated epigenetic markers such as alterations in DNA methylation patterns or post-translational modifications of histones, like methylation or acetylation(Fraga and Esteller 2007). Such epigenetic alteration may contribute to aging through mechanisms such as impinging DNA repair and genome stability, or through transcriptional alterations(López-Otín et al. 2013)

Loss of proteostasis

On the one hand, protein homeostasis includes the correct folding and subsequent stabilization of proteins. On the other hand, also protein degradation mechanisms by the proteasome or the lysosome need to be maintained to prevent accumulation and aggregation of damaged proteins. Impaired proteostasis contributes to the development of age-related pathologies like Alzheimers' and Parkinsons' disease(Powers et al. 2009, Koga et al. 2012).

Deregulated nutrient sensing

Mice treated with rapamycin showed extended longevity. Rapamycin mimics a state of limited nutrient availability, supporting the theory that decreased nutrient signalling in the course of dietary restriction (DR) increases lifespan and/ or healthspan in eukaryotes(Harrison et al. 2009). The pathway involved is the insulin and insulin-like growth factor (IGF-1) signalling (IIS) pathway, which ranks among the most conserved aging-controlling pathways(Barzilai et al. 2012a).

Mitochondrial dysfunction

The linkage between mitochondrial dysfunction and aging is not entirely clear. Various reports show that the increased amount of reactive oxygen species (ROS), as a result of age-related mitochondrial dysfunction, did not accelerate aging but to a certain extent functions more as a stress-elicited survival signal(Hekimi et al. 2011). Nevertheless, aged mitochondria become progressively insufficient and the efficacy of the respiratory chain tends to diminish, resulting in electron leakage and reduced adenosine triphosphat (ATP) generation(Green et al. 2011). This leads to an excessive ROS production, increased oxidative damage and mitochondrial mutations, which promote the aging process(Payne and Chinnery 2015).

Cellular senescence

As first described by Hayflick and Moorhead in 1961, cells do not have unlimited replicative potential and finally enter a state of irreversible growth arrest(HAYFLICK and MOORHEAD 1961). Beside telomere shortening, other aging-associated stimuli induce senescence, like non-telomeric DNA damage and de-repression of the p16/INK4/ARF locus, which seem to occur more frequently with increasing age(Collado et al. 2007). Cellular senescence is often considered as a protective mechanism to prevent further proliferation of damaged and potentially oncogenic cells. Senescent cells must be replaced by “young” cells, otherwise they accumulate and impair tissue homeostasis and therefore contributing to the aging process(López-Otín et al. 2013). In addition, senescent cells manifest a pro-inflammatory so called “senescent-associated secretory phenotype” (SASP)(Rodier and Campisi 2011). It includes elements like cytokines, growth factors as well as proteases(Coppé et al. 2010, Freund et al. 2010). They can have various effects on surrounding cells and tissues like inducing cell proliferation(Yang et al. 2006) and/or epithelial-to-mesenchymal transition(Laberge et al. 2012), stimulation of angiogenesis(Coppé et al. 2006) as well as alteration of stem cell proliferation and differentiation(Krtolica et al. 2011). Furthermore, some of the SASP factors promote inflammation, which is a concomitant feature of nearly every age-related disease and finally they may lead to accelerated aging(Franceschi 2007, Davalos et al. 2010).

Stem cell exhaustion

Stem cell exhaustion for instance caused by telomere shortening and/ or decreased cell cycle activity may results in a declined regenerative potential of tissues, as it is the case in immunosenescence(Rossi et al. 2008). Thereby haematopoiesis declines with age, which causes a diminished production of adaptive immune cells, a characteristic feature of aging(Shaw et al. 2010). Stem cell exhaustion can be found in most of the adult stem cell compartments of mice and is one of the most distinct evidence of aging(Molofsky et al. 2006)

Altered intercellular communication

The aging process has a strong influence on intercellular communication. Pro-inflammatory phenotypes, resulting from alterations in intercellular communication, are associated with age related diseases such as diabetes type 2 and contribute to the aging process(Barzilai et al. 2012b, Salminen et al. 2012) Another example of “contagious aging” is the phenomenon that senescent cells are able to induce senescence in neighbouring cells via gap junctions(Nelson et al. 2012).

1.1.2 Skin aging

1.1.2.1 The structure of human skin

The human skin is a huge organ composed of two main layers that blend into each other: epidermis and dermis (Fig.2). Its thickness varies a lot depending on the different parts of the body. The main functions of the skin are the homeostasis of the body temperature, oxygen uptake and barrier function. To guarantee all these features it is important that the hierarchical structure of the skin is maintained(Ulfig 2005).

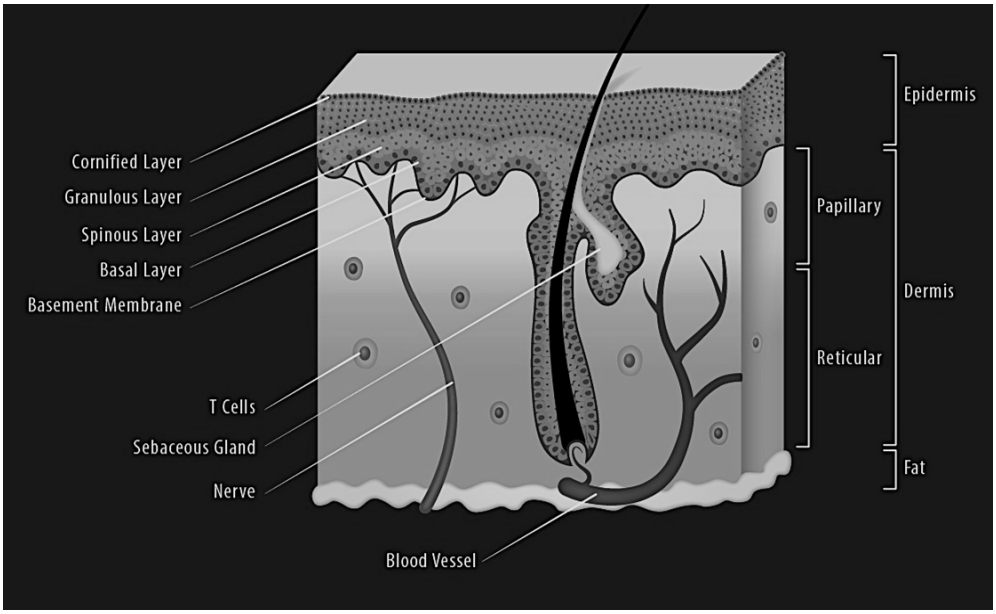

Figure 2: Structure of the human skin. Adapted from LifeMap Sciences('Skin Structure infographic - LifeMap Discovery')

Epidermis

The epidermis is the outermost part of the skin, organized in a stratified epithelium consisting of five layers, from the bottom to the top *Stratum basale, Stratum spinosum, Stratum granulosum, Stratum lucidum* and *Stratum corneum*(Ulfig 2005). It is mainly comprised of keratinocytes, which form a squamous epithelial layer serving as a protective waterproof barrier. Cells obtain their nutrients from the underlying dermis, as no blood vessels are present in the epidermis. Directly above the dermal-epidermal junction proliferating basal cells reside and build up the basal layer, a single cell layer from which the keratinocytes arise via mitosis('Anatomy and Physiology' 1362). As the keratinocytes migrate through all the different epidermal layers towards the skin surface they gradually differentiate into protein-enriched corneocytes, finally embedded in a lipid-rich extracellular matrix. This most superficial, impermeable barrier also known as *Stratum corneum*, is composed of 15 to 30 layers of cornified cells, which ensure mechanical protection and prevent penetration of microbes and dehydration(Elias et al. 1977, Rittie and Fisher 2015).

Dermis

The dermis is located directly below the epidermis and contains connective tissue, sweat glands and hair follicles. It is anchored to the Stratum basale via intertwining collagen fibers forming dermal papillae('Anatomy and Physiology' 1362). The dermal fibroblasts, which belong to the family of mesenchymal cells, regulate the metabolism of the extracellular matrix (ECM) through synthesis and degradation of ECM components like collagens and elastin.(Gunin et al. 2011)

The dermis can be separated into two layers. The *Stratum papillare* (papillary dermis) contains fibroblasts, collagen and elastic fibres, blood vessels and cells of the immune system. Characteristically it is arranged into dermal papillae, which are ridge-like structures extending the surface area of the epithelial-mesenchymal interaction and facilitate the exchange of soluble molecules(Sorrell and Caplan 2004). Papillary fibroblasts regulate hair follicle growth and arrector pili muscles(Driskell et al. 2013).

Linked below a vascular plexus – the *rete subpapillare* – extends the *Stratum reticulare* (reticular dermis) to the *rete cutaneum*. This deeper vascular plexus represents the boundary between dermis and hypodermis(Sorrell and Caplan 2004). The reticular dermis hosts only few cells but contains thick, strong bundles of collagen and elastic fibres that ensure the elasticity as well as the tear strength of the skin enabling movement.(Ulfig 2005). Furthermore the collagen fibres bind water and keep the skin hydrated.

Hypodermis/Subcutis

Comprised of fat and connective tissue, the *Subcutis* connects the skin with the underlying tissues. It is rich in adipocytes and its main function is to serve as isolation and thus to maintain the body temperature. The hypodermis varies in its composition depending on age, sex and diet. Often, hair follicles with their associated dermal cells extend into this deep located layer(Ulfig 2005).

1.1.2.2 Papillary and Reticular fibroblasts – What are the differences?

Fibroblasts in the skin represent a heterogeneous population composed of papillary and reticular fibroblasts located in the papillary and reticular dermis(Sorrell and Caplan 2004), respectively with distinct characteristics(Sorrell et al. 2004). By dermatoming skin samples these two cell populations can be separately isolated and examined.

Papillary fibroblasts were assigned as thin, spindle-shaped cells, exhibiting an increased proliferation capacity. When cultivated in monolayer cultures, they seemed to be not fully contact inhibited and therefore reach higher cell density(Sorrell et al. 2004). Reticular fibroblasts appear more flattened and wide-spread and typically express more α-smooth muscle actin (α-SMA), a marker for myofiboblasts(Janson et al. 2012). They also induce faster contraction of type I collagen lattices(Sorrell et al. 1999) indicating a function in wound healing. Fitting to those observations is the fact that reticular fibroblasts overexpress genes involved in cell motility, whereas papillary fibroblasts show increased expression of genes important in immune response(Janson et al. 2012).

Fibroblasts influence keratinocyte behaviour by the release of growth factors. Two of the most important mesenchyme-derived factors regulating keratinocyte proliferation and influencing wound healing are keratinocyte growth factor (KGF) 1 and granulocyte-macrophage colony stimulating factor (GM-CSF)(Rubin et al. 1995, Werner and Smola 2001). Papillary fibroblasts secret a higher ratio of GM-CSF to KGM-1 compared to reticular fibroblasts(Sorrell et al. 2004). Interestingly, overexpression of KGF-1 facilitates hyperproliferation of the keratinocytes(Andreadis et al. 2001), whereas overexpression of GM-CSF leads to increased apoptosis of epidermal cells(Breuhahn et al. 2000). This implies that these two fibroblast populations influence epidermal proliferation and differentiation in variable extent and that a finely tuned balance between pro- and anti-proliferative signals needs to be maintained to accomplish epidermal homeostasis.

1.1.3 Age related skin phenotypes

Beside the genetic background also other factors like epigenetic mechanisms and the environment have a strong influence on the aging process(Macieira-Coelho 1997). Cells are continuous exposed to exogenous and endogenous DNA damaging agents, such as ultraviolet radiation (UV) as well as reactive oxygen species, which can cause DNA damage in all phases of the cell cycle(Kakarougkas and Jeggo 2014). Failure of DNA damage response (DDR) promotes pathophysiological outcomes such as cancer, hereditary disorders as well as premature ageing(Garinis et al. 2008, Dellago et al. 2012, Mahajan 2015). But if the mammalian cell response works properly after DNA damage multiple protein complexes coordinate and act together to facilitate the restoration of the genomic integrity(Motoyama and Naka 2004, Howard et al. 2015). They do so by activating DNA damage checkpoint pathways that initiate signalling cascades resulting in cell cycle arrest as well as recruitment of damage specific repair complexes(Kakarougkas and Jeggo 2014).

During aging, striking, changes can be observed in human skin such as wrinkles, irregular pigmentation and reduction in thickness, but also a decreased capacity for adaptive responsiveness and wound healing, resulting in an enhanced risk of disorders and death. On a molecular and histological level, chronologically and photo–aged skin, in contrast to intact, young skin, exhibits a reduced and disorganized collagenous extracellular matrix concomitant with a flattened dermal-epidermal junction(Rittie and Fisher 2015)(Mine et al. 2008). Furthermore, skin aging is reflected by atrophy, loss of elasticity and loss of the rete ridges by retraction of the dermal connective tissue(Montagna and Carlisle 1979, Lavker et al. 1987). Figure 3 illustrates some of these histological changes in the human skin.

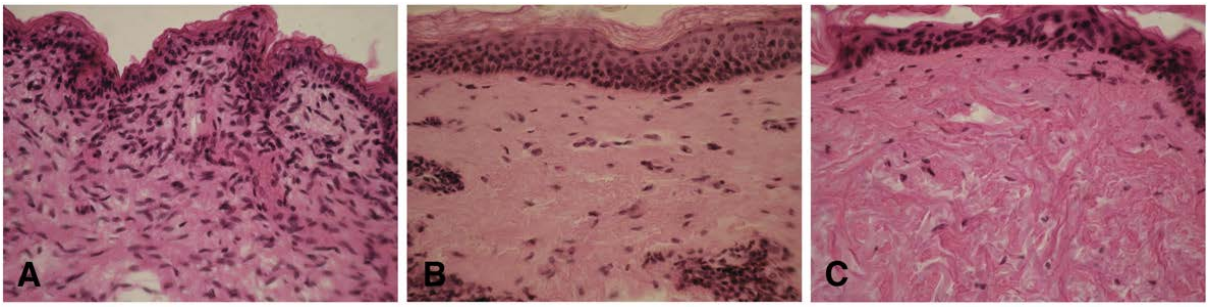

Figure 3: Histological skin sections of different age..(A) Sample from 33 week male fetus. (B) Sample from 52 years old man. (C) Sample from 77 years old man. Skin sections were immunohistochemicaly stained for proliferating cell nuclear antigen (PCNA). Adapted from Gunin et al. (2014)(Gunin et al. 2014)

Aging in general and skin aging are non-preventable but modulatable processes resulting from intrinsic and extrinsic factors leading to changes in the cellular homeostasis. It is interesting that there seems to be a difference in the protein profile of aged-skin phenotypes caused by intrinsic and extrinsic factors(Fang et al. 2016). This makes aging an even more complicated and sophisticated topic in contemporary research.

1.1.3.1 Papillary to Reticular transition

As already mentioned before the dermis consists of two parts: papillary and reticular dermis, hosting two different types of fibroblasts(Sorrell and Caplan 2004). Subpopulations of papillary and reticular fibroblasts exhibit different characteristics for example regarding cellular morphology, proliferation rate and ECM production potential(Harper and Grove 1979, Azzarone and Macieira-Coelho 1982). During aging the human skin undergoes several changes like the progressive decrease of tissue thickness including the loss of epidermal ridges(Lavker et al. 1987)(Janson et al. 2013). The fact that there are changes in the cellular composition of the human dermis during the aging process may be a reason(Janson et al. 2013).

Additionally to signs of senescence, high-passage papillary fibroblasts decrease their expression of the papillary marker podoplanin (PDPN) but increase their expression of the reticular marker genes transglutaminase (TGM) 2, calponin (CNN) 1 and α-SMA after prolonged culture compared to low-passage papillary cells(Janson et al. 2013). The characteristic spindle-shaped morphology gets lost with increased age and the cells remind more of reticular fibroblasts(Mine et al. 2008). Furthermore, the higher growth rate typical for young papillary fibroblasts, as well as the increased potential to promote epidermal morphogenesis compared to reticular fibroblasts diminishes with higher age and becomes similar in both subpopulations(Mine et al. 2008). Whereas, the secretion profile of reticular fibroblasts is similar in low and high passages, the protein secretion of papillary fibroblasts adjusts to the one of the reticular subpopulation with increasing age, meaning and increase in secretion levels of growth factor KGF, metalloproteinase (MMP)-1, 2 and 3 as well as metalloproteinase inhibitor (TIMP)-1 and 2(Mine et al. 2008). Interestingly, in reticular fibroblasts there is no significant change in the expression of marker genes(Janson et al. 2013) and very little to no change in morphology, proliferation rate and protein secretion profile(Mine et al. 2008). The reason for the decline in the papillary dermis of aged skin might be caused by the reduced growth potential and altered secretion profile of high-passage papillary fibroblasts leading to structural changes in dermal and epidermal tissue, suggesting the assumption that a papillary to reticular transition (PRT) takes place during aging. As shown in Figure 4, papillary fibroblasts might be more affected by aging as reticular fibroblasts, representing the central anchor in the PRT process(Mine et al. 2008).

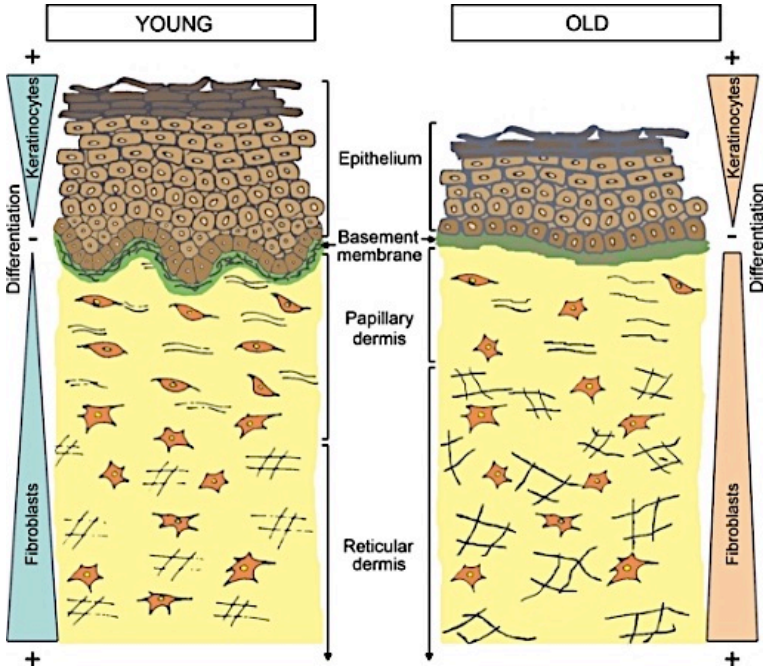

Figure 4: Papillary to reticular transition in human skin aging. During the process of aging the human dermis as well as the epidermis are subjected to structural and physiological changes mainly due to the modifications of papillary fibroblasts. Thus cellular differentiation is impaired and may alter the hierarchical cellular organization. Adapted from Mine, S. et al. (2008)(Mine et al. 2008)

1.1.4 Wound healing and alterations during aging

There are two different forms of wound healing: reparative and regenerative wound healing. In reparative healing the wound heals with scarring and without reformation of skin appendages like hair follicles(Woodley 2017). In contrast to mammals some lower animals like the newt are capable to regrow an entire new functional limb once cut of. This is facilitated by regenerative wound healing(Donaldson et al. 1987). A similar phenomenon was observed in foetuses. Within the first trimester of gestation they are able of scar less skin wound healing(Longaker and Adzick 1991). Human skin wounds heal largely by reparative wound healing, which is immediately induced after wounding and can be divided in three phases. In the inflammatory phase a blood clot fixes the lesion in the capillary and recruits inflammatory cells like neutrophils and macrophages and also fibroblasts as well as

endothelial cells into the wounded area. In the proliferative phase angiogenesis takes place, which is critical for the proliferation of fibroblasts(Epstein et al. 1999). In the emerging granulation tissue fibroblasts differentiate and modulate into contractile myofibroblasts expressing α-smooth muscle actin, important in wound contraction and re-epithelialization(Hinz and Gabbiani 2003). The maturation and scar formation are part of the resolution phase, in which the granulation tissue is remodelled through proteolytic enzymes, MMPs and their inhibitors. Finally, at the end of the healing process myofibroblasts and vascular cells are reduced by apoptosis(Darby et al. 2014). During these phases of wound healing keratinocytes, fibroblasts and endothelial cells need to undergo three important processes orchestrated by epidermal-mesenchymal interactions(Woodley 2017). To ensure “reepithalization” keratinocytes must be reprogrammed into motile cells migrating laterally across the wound bed. Then periwound fibroblasts migrate into the clot to transform it into neodermis by producing collagen and other ECM compounds. This process is called fibroplasia. In the proliferative phase of wound healing neovascularization by periwound microvascular endothelial cells needs to occur to re-establish normal blood supply(Woodley et al. 2015). New neodermis in full thickness wounds is mainly comprised of reticular fibroblasts. This fibroblast linage is not able to promote hair follicle growth but boosts the synthesis of collagen, suggesting that reticular fibroblasts are largely involved in ski wound healing rather than papillary fibroblasts(Woodley 2017).

The relation between increased age and the occurrence of chronic wounds was first described in medical literature more than one hundred years ago(Du Noüy 1916). The effect of increased age on wound healing is mainly a temporal decline rather than worse quality of healing(Ashcroft et al. 1997). Cumulative potentialy deleterious effects alter the skin physiology like for example they lead to a flattening of the dermal-epidermal junction. This makes aged skin more susceptible to separation of the two skin layers resulting in partial thickness skin injuries such as skin tears(Pittman 2007). Also the three phases of inflammation exhibit changes with aging like a decreased amount of growth factors, diminished cell proliferation and migration as well as ECM synthesis(Gosain and DiPietro 2004). The macrophage function, especially important in the inflammatory phase, is decreased in the elderly(Ashcroft et al. 1997). The decreased number, size and proliferation rate of dermal fibroblasts leads to delayed wound closure, which in turn increases the risk of infections(Grove and Kligman 1983, Bruce and Deamond 1991). Additionally, incisional

wounds of older people display a lower tensile strength compared to that of younger ones(SANDBLOM). When taken as a whole, there are characteristic changes affecting the process of wound healing in aged individuals compared to young ones.

1.2 The human protein *SNEV/PSO4/PRPF19*

1.2.1 The structure of *SNEV/PSO4/PRPF19*

ScPSO4 was first identified in *Saccharomyses cervisiae* as a psoralen-sensitive mutant 4 as it was unable to repair photoactivated 8 methoxy psoralen-induced DNA-interstrand crosslinks (ICL) and was found to be allelic to prp19 in haploid cells and crucial for mRNA splicing(da Silva et al. 1995, Grey et al. 1996).

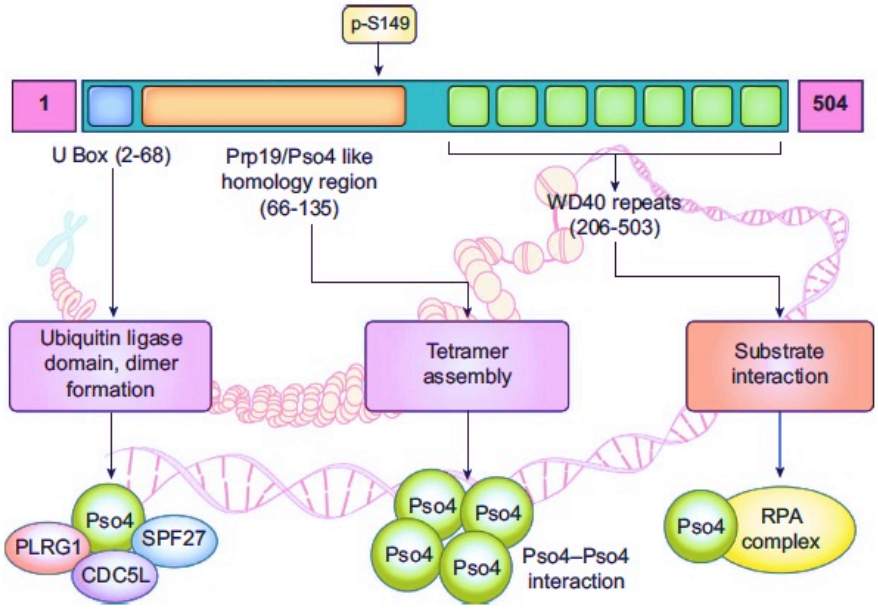

Figure 5: Schematic illustration of the structure of *SNEV*.

Adapted from Mahajan, K. (Mahajan 2015)

The human ortholog *PSO4/PRPF19* has been discovered as a multi-talented protein playing a role as part of the nuclear matrix (hNMP200)(Gotzmann et al. 2000), DNA repair factor (hPso4)(Mahajan and Mitchell 2003), senescence evasion factor (SNEV)(Grillari et al. 2005), essential mRNA splicing factor (Prp19)(Chan et al. 2003) and it is involved in the ubiquitin/proteasome pathway exhibiting a enzymatic activity as an E3 ubiquitin ligase(Hatakeyama and Nakayama 2003) and direct proteasome interaction(Löscher et al. 2005). It is located on chromosome 11q12.2 and ubiquitously expressed in humans. As

illustrated in Figure 5, *SNEV* (from now on termed like this) is a 55-kDa protein comprised of a N-terminal U-box(Vander Kooi et al. 2006), a central coiled-coil Prp19 homology region(Ohi et al. 2005) and seven-bladed WD40 β-propeller type leucine-rich repeats forming an asymmetric barrel-shaped structure(Ohi et al. 2005, Vander Kooi et al. 2010). The three major structural parts display different functions. The U-box is a catalytic domain, which shows E3 ubiquitin ligase activity stimulating poly-ubiquitination of target proteins(Pickart 2001). Normally, ubiquitination creates a proteolytic signal via an enzyme cascade composed of activation (E1), conjugation (E2) and ligation (E3) enzymes, which mark proteins for degradation by the proteasome. But it can also play a regulatory role as it is the case in $SNEV^{hPrp19/hPso4}$ (Chanarat and Sträßer 2013), (Pickart 2001). A mutation within its U-box can result in mRNA splicing defects(Chen et al. 1998, Ohi and Gould 2002). The central coiled-coil Prp19 homology region regulates sufficient tetramer formation in the splicosome(Ohi et al. 2003) whereas, the WD40 β-propeller type leucine-rich repeats show scaffolding function by substrate recognition as well as recruitment(Grote et al. 2010), (Tarn et al. 1994). *SNEV* can be found in different protein complexes involved in several molecular mechanisms like DNA repair, ubiquitination and transcription.

1.2.2 The function of *SNEV/PSO4/PRPF19* and its interaction partners

SNEV is a ubiquitously expressed, multitalented protein identified during the investigation of variations in the gene expression pattern of replicative senescent versus early passage HUVECs(Grillari et al. 2000). It is involved in diverse cellular pathways and interacts with several components (Table 1).

Table 1. Functions and interactions of *SNEV*

Cellular Process	Function of *SNEV*	Interaction
Splicing	Stable splicosomal assembly and activation.	Cdc5L Splicing factors
DNA Repair	• DSB repair • ICL repair • Replication stress response • Interaction with damage checkpoint kinases	ds-DNA Prp19 core complex RPA ATM
Apoptosis and Life Span Regulation	Enhancing capacity of DDR and/or resistance to stress.	ATM
Transcription	Linkage of splicing and DNA repair.	XAB2 THO

Splicing and Ubiquitination

Splicing is an important process removing introns and ligating exons from pre-mRNA. The splicosome consists of five small nuclear ribonucleoproteins (snRNPs) and several non snRNP splicing factors like SNEV$^{hPrp19/hPso4}$ (Will and Luhrmann 2011). In the splicosome *SNEV* is found in a subcomplex termed the hPrp19/cell division cycle 5 protein (Cdc5L) complex. It plays a key role during splicosomal assembly and activation as it accomplishes structural support and stabilizes the association of U5 and U6 snRNPs with the pre-mRNA(Chan and Cheng 2005). The coupling of the hPrp19/Cdc5L complex to the activated splicosome and the 35S from U5 is required for both steps of splicing(Makarov et al. 2002, Makarova et al. 2004, Deckert et al. 2006). Moreover, *SNEV* interacts in synergy with several different splicing factors such as Blom7α and Exo70, modulating splicing activity(Grillari et al. 2009), (Dellago et al. 2011).

The molecular mechanism of *SNEV* in the splicosome depends on its U-box with E3 ubiquitin ligase activity(Yin et al. 2012). K63-linked poly-ubiquitin chains increase the binding affinity of

Prp3, a component of the U4 snRNP, for the Prp8 component of the U5 snRNP. This leads to the structural stabilization of U4/U5.U6 snRNP. Dissociation of U4 from the splicosome is accomplished via its deubiquitination by the Usp4/Sart3 deubiquitination enzyme(Song et al. 2010).

DNA Repair

Our DNA is constantly exposed to exogenous and endogenous agents capable to induce DNA damage in form of interstrand crosslinks (ICL), single-strand breaks (SSB) and double-strand breaks (DSB). After DNA damage, DNA damage checkpoint pathways are activated resulting in cell cycle arrest and the recruitment of specific DNA damage response (DDR) protein complexes facilitating for example homologous recombination, non-homologous end joining (NHEJ), alternative-NHEJ and ICL repair(Kakarougkas and Jeggo 2014).

SNEV binds double stranded DNA after activation of DDR pathways and facilitates processing as well as repair of DNA lesions(Zhang et al. 2005). Interestingly, on the one hand *SNEV* overexpression is connected to a protective effect against DNA-damage induced cell death(Lu and Legerski 2007). On the other hand, a loss of its expression evokes an increase in sensitivity to DSB-forming agents like ionizing radiation and mitomycin C(Mahajan and Mitchell 2003). Thus, *SNEV* is involved in the DDR machinery, being specifically recruited to the site of damage.

ICLs act as blockers of DNA replication fork progression, which affects cell viability. As already mentioned, *SNEV* plays a crucial role in DNA ICL repair pathways as it is part of the Prp19 core complex. In this complex it shows the strongest interaction with Cdc5L(Zhang et al. 2005). A possible molecular explanation how this complex is involved in ICL repair comes from the observation that Cdc5L binds to WRN protein(Zhang et al. 2005). WRN protein is defective in patients suffering from Werner Syndrome and exhibits a DNA helicase activity essential for homologous recombination and recombination of stalled replication forks. Induced by DNA damage *SNEV* evolves its double stranded DNA (ds-DNA) binding affinity and together with Cdc5L it stabilizes WRN helicase at ICLs(Mahajan and Mitchell 2003, Zhang et al. 2009). The importance of these functions is highlighted by the fact that Werner syndrome patients develop a segmental progeroid syndrome(Lee et al. 2005b, Chanarat and

Sträßer 2013). If interstrand crosslinks change into single stranded-gaps or DSB, *SNEV* may act as a docking site for other DDR pathways(Zhang et al. 2009).

Prolonged stalling of replication forks can result in replication fork collapse, SSBs and DSBs(Zhang et al. 2015). This leads to the activation of the ataxia telangiectasia mutated and Rad3 related (ATR)/checkpoint kinase 1 (Chk1)-dependant replication stress checkpoint pathways(Kaufmann 2010). Replication protein A (RPA), which is one of the first proteins binding single stranded DNA (ss-DNA) at stalled replication forks and hence, serving as a nucleation point for the binding of the DDR checkpoint complex, is a further interaction partner of *SNEV*(Mahajan 2015). *SNEV* colocalizes with proliferating cell nuclear antigen (PCNA)(Wan and Huang 2014), interacts with RPA and together they accomplish replication fork stability and/or restart(Lu and Legerski 2007). Furthermore, in response to camptothecin (CPT, a topoisomerase I inhibitor) *SNEV* can act as a component of the damage-sensing complex, acting together with RPA as a sensor in an ATR-dependant manner(Maréchal et al. 2014). It facilitates autophosphorylation of ATR and the recruitment of its obligatory partner ATR interaction protein (ATRIP) resulting in phosphorylation of its effectors such as Chk1(Maréchal et al. 2014, Wan and Huang 2014). The U box of *SNEV* is required for the ubiquitination of RPA, which facilitates the recruitment of ATRIP to the RPA-ssDNA complex and thus, ATR activity is enhanced(Maréchal et al. 2014).

ATM, the protein encoded by the ataxia telangiectasia mutated gene, is a member of the phosphatidylinositol 3-kinase (PI3KI) family and appears as an inactive dimer in healthy cells(Álvarez-Quilón et al. 2014). Its crucial role in coordinating different cellular responses to DSBs is emphasized by the fact that biallelic mutations in the human ATM gene can lead to adverse effects like DNA repair defects and altered cell cycle checkpoint activation(Lim et al. 2000, Paull 2015). Upon DNA damage, ATM undergoes autophosphorylation, is activated in a Mre11-Rad50-Nb1 (MRN)-dependant manner and functions as a serine/threonine protein kinase of numerous downstream targets, eliciting the DNA damage response(Bakkenist and Kastan 2003, Berkovich et al. 2007, Álvarez-Quilón et al. 2014, Paull 2015). Subsequently, on one hand, cell cycle checkpoints like G1/S checkpoint(Kastan and Lim 2000), intra-S-phase and G2/M checkpoints are prominent targets that get activated(Xu et al. 2002). On the other hand, ATM is necessary to facilitate the relaxation of heterochromatine, which enables

repair proteins to access sites of DNA double-strand breaks(Shackelford et al. 2001). In response to oxidative stress *SNEV* is phosphorylated at serine 149 (S149) by ATM and this phosphorylation is required to exert its function in protecting from apoptosis and increasing efficiency of DNA damage repair (Dellago et al. 2012). The respective molecular mechanism has not yet been resolved.

Apoptosis and Life Span Regulation

Moreover *SNEV* regulates replicative senescence in mammalian cells and has therefore been named as such: senescence evasion factor(Voglauer et al. 2006). A depletion of *SNEV* in HeLa cells results in the accumulation of apoptosis(Zhang et al. 2005) whereas, the overexpression in human cells revealed a pro-survival effect upon DNA damage(Lu and Legerski 2007). It was shown by Voglauer et al that an overexpression of wild type *SNEV* mediates the resistance to apoptosis and extends the replicative live span of HUVECs(Voglauer et al. 2006). The life span prolonging phenomenon depends partially on the phosphorylation of *SNEV* by ATM whereas, the apoptosis resistance is stringently linked to this process(Dellago et al. 2012). The fact that *SNEV* is involved in the regulation of replicative senescence is supported by the fact, that a deletion of the gene is lethal in embryonic mice(Fortschegger et al. 2007).

Transcription

Transcription can be seen as the mechanism that possible couples splicing and DNA repair in a bidirectional way, ensuring that only proper spliced mRNA is released into the cytoplasm(Martins et al. 2011). Additionally, it may also influence some DNA repair pathways(Tornaletti 2009). *SNEV* together with other splicing factors is associated with a multimeric RNA-binding complex containing XAB2 (XPA-binding protein, where XPA stands for xeroderma pigmentosa group A protein, which is involved in nucleotide excision repair and transcription-coupled repair (TCR))(Nakatsu et al. 2000, Ding et al. 2012). After deleterious exposure to UV the interaction of XAB2 with XPA and following, DNA repair is enhanced(Kuraoka et al. 2008). A similar effect could be observed investigating the interaction of XAB2 with RNA polymerase II, which is also increased after UV, cisplatin and mitomycin C treatment(Kuraoka et al. 2008). Moreover *SNEV* interacts with THO a subcomplex of the transcription export (TREX) complex in yeast(Chanarat et al. 2011). It

couples transcription to nuclear export and therefore influences genome maintenance(González-Barrera et al. 2002). A depletion of the THO complex in human cells leads to DNA breaks resulting in hyper-recombination(Domínguez-Sánchez et al. 2011).

In sum, *SNEV* is an essential protein involved in several complex molecular mechanisms, affecting human physical health and the phenomenon of aging.

2 Aim of the study

The object of this thesis was to further characterize the human protein *SNEV*. We wanted to investigate its role in skin functionality and skin aging. More specifically, the aims of the study were:

On the one hand, we aimed to establish stable *SNEV* overexpressing fibroblast cell lines, including a phosphorylation-mutant-*SNEV* overexpressing cell line to investigate the effect of a lack of *SNEV* phosphorylation.

We wanted to characterize the stable transduced fibroblast cell lines with respect to their cellular morphology, growth, cellular senescence, their communication with epidermal keratinocytes and wound healing.

On the other hand, we aimed to establish and characterize stable *SNEV* overexpressing human epidermal keratinocytes

3 Material and Methods

3.1 Materials

3.1.1 Disposables

Table 2. Disposables used

Material	Manufacturer
Falcon tubes, Cellstar® (15 mL, 50 mL)	Greiner Bio-one, Kremsmünster (A)
CryoTube vials	Thermo Scientific, Waltham (USA)
Filter unit, 0.45 µm, Millex GP Filter unit	Merck, Darmstadt (D)
Filter unit, 0.22 µm, Millex GP Filter unit	Merck, Darmstadt (D)
Gloves, Semper Care Premium	Semperit, Wien, (A)
Micro tubes, 1.5 mL, sterile	Sarsted, Nürnbrecht (D)
Micro tubes, 2.0 mL, sterile	Sarsted, Nürnbrecht (D)
Pipette, Cellstar®, serological (2 mL, 5 mL, 10 mL, 25 mL, 50 mL)	Greiner Bio-one, Kremsmünster (A)
PCR tubes, 8-tube strips, 0.2 mL	Biozyme, Wien (A)
Pipette tips (100 µL, 200 µL)	Greiner Bio-one, Kremsmünster (A)
Pipette tips (10 µL)	Starlab, Hamburg (D)
RNase Zap wipes	Ambion, Carlsbad (USA)
Roux flasks (25 cm^2, 75cm^2, and 175cm^2)	Greiner Bio-one, Kremsmünster (A)
24-well plates, Nunclon Delta Surface	Thermo Scientific, Waltham (USA)
12-well plates, Nunclon Delta Surface	Thermo Scientific, Waltham (USA)
6-well plates, Nunclon Delta Surface	Thermo Scientific, Waltham (USA)
15 µ-Slide 8 Well	IBIDI, Martinsried (D)

3.1.2 Laboratory equipment

Table 3. Laboratory equipment

Equipment	Model	Manufacturer
Cell Counter	Vi-Cell® XR	Beckmann Coulter, Brea (USA)
Centrifuge	Centrifuge 5415 R	Eppendorf, Hamburg (D)
	Centrifuge 5810 R	Eppendorf, Hamburg (D)
	Centrifuge 5804 R	Eppendorf, Hamburg (D)
	Laboratory Centrifuges 4–15	Sigma, Osterode am Harz (D)
	VWR™ Galaxy Mini Microcentrifuge	VWR™ International, Pennsylvania (USA)
Gel Imager	Odyseey Infrared Imager	Li-Cor, Lincoln (USA)
Incubator (Cell culture)	Heraeus BBD cytoperm 2 Heracell 150i CO^2 Incubator	Thermo Scientific, Waltham (USA) Thermo Scientific, Waltham (USA)
Laminar hood	HBB2448 LaminAir	Holten, Hanau (D)
Microscope	CK2	Olympus, Shinjuku (J)
	DFC 425 C	Leica, Wetzlar (D)
	KL 300 LED	Leica, Wetzlar (D)
	DM IL LED	Leica, Wetzlar (D)
PCR cycler	T3 Thermocycler	Biometra, Göttingen (D)
pH-meter	pH 521	WTW, Weilheim (D)
Plate shaker	IKA Vibrax-VXR, Typ VX7	IKA, Staufen (D)
Pipettes	Research Plus, 100–1000 µL	Eppendorf, Hamburg (D)
	Research Plus, 20–200 µL	Eppendorf, Hamburg (D)
	Research Plus, 2–20 µL	Eppendorf, Hamburg (D)
	Research Plus, 0.5–10 µL	Eppendorf, Hamburg (D)
	Research Plus, 0.1–2 µL	Eppendorf, Hamburg (D)
RT-qPCR cycler	Rotor-Gene-Q	Qiagen, Venlo (NL)
Recirculating Cooler	F250 Recirculating Cooler	Julabo, Seelbach (D)
Spectroscope	NanoDrop One	Thermo Scientific, Waltham (USA)

Radiation Unit	Sellamed 1200	Sellas Medizinisch Geräte GmbH, Gefelsberg (D)
Thermomixer	Thermomixer comfort	Eppendorf, Hamburg (D)
	Thermomixer C	Eppendorf, Hamburg (D)
Vortex Mixer	VF2	IKA, Staufen (D)
Water bath	Water bath	GFL, Bergwedel (D)

3.1.3 Chemicals and Reagents

Table 4. Chemicals and Reagents

Chemical/Reagent	**Manufacturer**
β-gal Staining Kit	Invitrogen, California (USA)
Blasticidin	InvivoGen, California (USA)
Bovine Serum Albumin	Sigma-Aldrich, Missouri (USA)
Calcium Chloride Solution	Sigma-Aldrich, Missouri (USA)
Chloroform	Sigma-Aldrich, Missouri (USA)
Citric Acid Monohydrate	Sigma-Aldrich, Missouri (USA)
Collagen G (bovine)	Merk Millipore, Darmstadt (D)
DMSO	Sigma-Aldrich, Missouri (USA)
Derma Life Basal Medium	Life Line Cell Technology, Maryland (USA)
Deoxynucleotide dNTPs	New England Biolabs, Massachusetts (USA)
Distilled Water	Life Line Cell Technology, Maryland (USA)
Dulbecco's Modified Eagle Medium/Ham's F12 (1:1)	Biochrom, Merk Millipore, Darmstadt (D)
Ethanol 99.9 %	Merk Millipore, Darmstadt (D)
FavorPrep GEL/PCR Purification MiniKit	Favorgen Biotech Corp. (TWN)
Fetal Calf Serum	Sigma-Aldrich, Missouri (USA)
Formaldehyde 36 %	VWR™ International, Pennsylvania (USA)

Geneticin G418	InvivoGen, California (USA)
Glycerol for molecular biology ≥99 %	Sigma-Aldrich, Missouri (USA)
Glycoblue	Thermo Fisher Scientific, Massachusetts (USA)
GoTaq® G2 DNA Polymerase	Promega, Wisconsin (USA)
5x Green GoTaq Reaction Buffer	Promega, Wisconsin (USA)
High capacity cDNA Reverse Transcription Kit	Applied biosystems, California (USA)
Isopropanol	Merk Millipore, Darmstadt (D)
L-Glutamine	Sigma-Aldrich, Missouri (USA)
KGM™-2 Keratinocyte Growth Medium-2	Lonza, Basel (CH)
N-Acetyl NACL	Sigma-Aldrich, Missouri (USA)
NeoClear	Merk Millipore, Darmstadt (D)
Optimem	Thermo Fisher Scientific, Massachusetts (USA)
Penicillin/ Streptavidin	Sigma-Aldrich, Missouri (USA)
Phosphate Buffered Saline	Biochrom, Merk Millipore, Darmstadt (D)
Recombinant RNasin®	Promega, Wisconsin (USA)
Roti® Histofix 4%	Carl Roth, Karlsruhe (G)
Trizol TRI-Reagent	Sigma-Aldrich, Missouri (USA)
0.1% Trypsin/ 0.02% EDTA	Sigma-Aldrich, Missouri (USA)
Trypsin Inhibitor	Sigma-Aldrich, Missouri (USA)
Tween 20	Sigma-Aldrich, Missouri (USA)

3.2 Cell culture

3.2.1 Sterilization

Equipment that needed to be sterilized in-house was autoclaved at 121 °C for at least 20 minutes. Heat sensitive solutions (e.g. keratinocyte differentiation medium) were sterilized by filtration (0.22 µm pore size).

3.2.2 Cultivation of mammalian cells

Routine cell culture work was carried out in a laminar flow hood (Holten, Germany) to ensure a sterile work environment. The cells were cultured in roux culture flasks and multi-well plates in a humidified incubator (Thermo Scientific, USA) with 7 % CO_2 at 37 °C. Cells were passaged when they reached, depending on the cell line, a confluence between 60-90 % in a ratio reaching from 1:2 to 1:5 approximately twice a week.

For passaging, the spent culture medium was discard from the culture vessel and the cells were washed twice with Dulbecco's phosphate buffered saline (PBS) (Merck Millipore, Germany) without calcium and magnesium. To dissociate the cells from culture vessel they were incubated with 0.1 % trypsin and 0.02 % EDTA (Sigma-Aldrich, USA) in PBS for 5 min at 37 °C. After confirmation under the microscope that more than 90 % of the cells have detached, the cells were, to inhibit trypsin activity, re-suspended in an appropriate amount of culture media containing 10 % fetal calf serum (FCS) (Sigma-Aldrich, USA).

As keratinocytes are cultured in serum-free media they need an additional centrifugation step to get rid of the trypsin. After conformation of detachment trypsin inhibitor (Sigma-Aldrich, USA) was added to the cells and they were re-suspended in PBS. The cell solution was transferred into a 15 ml Falcon tube (Greiner Bio-one, Austria) and centrifuged at 170 x g for 5 min. The supernatant was discarded and the cell pellet re-suspended in an appropriate

amount of culture media. The cell solution was split into fresh culture vessels according to the desired split ratio. Table 5 illustrates the different amounts of media, PBS, dissociation reagent and trypsin inhibitor used for different culture vessels.

Table 5. Illustration of the different amounts of reagents depending on used culture vessel

Culture vessel	Surface area (cm^2)	PBS (mL)	Trypsin (mL)	Trypsin inhibitor (mL)	Volume of medium (mL)
12-well	3.8	0.5	0.5	0.5	1.5
6-well	9.4	1	0.5	0.5	2
T25	25	5	0.5	0.5	5-6
T75	75	5	1	0.5	15

3.2.3 Cell lines

3.2.3.1 Human diploid fibroblasts (HDF)

Human diploid fibroblasts were obtained from skin tissue samples. The cells were cultivated in Dulbecco's Modified Eagle Medium (DMEM) and Ham's F12 (1:1) (Merk Millipore, Germany), supplemented with 10 % FCS and 4 mM L-glutamine (Sigma-Aldrich, USA). HDFs were passaged when they reached about 90 % confluence in a split ratio 1:2 or 1:3 twice a week. The tree different donor cell lines used for various experiments were termed HDF85, HDF76 and HDF161.

3.2.3.2 Normal human epidermal keratinocytes (NHEK/SVTERT 3-5)

NHEK were isolated from human skin tissue. The cells had previously been transfected with a plasmid encoding SV40 early region followed by transfection with human telomerase reverse transcriptase (hTERT) to generate an immortal cell line. These cells were cultivated in keratinocyte growth media 2 (KGM-2) (Lonza, Switzerland) supplemented with 50 µg/mL Geneticin (G418) (InvivoGen, USA) as a selective agent. To avoid differentiation NHEK/SVTERT were passaged in a split ratio of 1:3 or 1:4 twice a week when they reached maximally 60 to 70 % confluence.

3.2.4 Cryopreservation – freezing and thawing cells

The longer cells are kept in culture, the more prone they are to undergo genetic drift or to get hit by mutations. To preserve structurally intact living cells, cryopreservation in liquid nitrogen is a commonly used method. As unprotected freezing in most cases is lethal for the cells, cryoprotectants are added to the media before freezing. They penetrate the cells, increase the concentration of all solutes in the system by reducing the intracellular water content and by that reduce the formation of ice crystals at any given temperature. There are several different cryoprotectants on the market such as Dimethyl sulfoxide (DMSO), which was the reagent of choice for all cell lines mentioned above. To further minimize the damage occurring to the cells during freezing, CryoTube vials (Thermo Scientific, USA) were labelled and pre-cooled to -80 °C. Cultured cells should be frozen at a passage number as low as possible, in a high concentration and the viability before freezing should be at least 90 %. In our case usually 25 cm^2 cells were frozen into one CryoTube vial. De facto one T75 roux culture flask was frozen into three cryotube vials.

To freeze the cells they were harvested by trypsinization as described previous in section 3.2.2. In order to get rid of the trypsin before freezing down the cells the re-suspended cell solution was centrifuged at 170 x g for 5 min. Supernatant containing the trypsin was removed and the cell pellet re-suspended in 1 mL pre-cooled cryo medium per CryoTube

vial. The cryo medium for fibroblasts was composed of DMEM/Ham's F12 (1:1) supplemented with 10 % FCS, 4 mM L-glutamine and 10 % DMSO (Sigma-Aldrich USA). For keratinocytes it consists of KGM-2 supplemented with G418 and 10 % DMSO.

Cells re-suspended in cryo medium were aliquoted and 1 mL was transferred into each pre-cooled CryoTube vial. Subsequently the vials were stored at -80 °C for at least 24 h to ensure a slow and gentle freezing. Then the frozen cells were transferred into liquid nitrogen tanks and stored at the gas phase above the liquid nitrogen.

For subsequent thawing a good technique and quick working is essential as this procedure is very stressful to frozen cells. The CryoTube vials were transferred from the liquid nitrogen direct into a tube filled with ethanol (Merck Millipore, Germany) to thaw the cells and then further warmed by hand. The unfrozen cell suspension was diluted with appropriate pre-warmed medium to reduce the toxic effects of the DMSO. Following a 5 minutes centrifugation step at 170 x g the supernatant was discarded to remove the cryoprotectant. The cell pellet was re-suspended in growth media and transferred into a respective culture vessel. After 24 h of cultivation the culture medium was replaced by fresh medium in order to remove dead cells.

3.2.5 Cell counting

To seed a specific number of cells per square centimetre the cell number needs to be determined. Cells were incubated with 0.1 % trypsin and 0.02 % EDTA in PBS for 5 min at 37 °C, after two initial washing steps, to detach from the cultivation vessel. After conformation of detachment under the microscope the cells were re-suspended in the appropriate culture media and one millilitre was transferred into a Vi-CELL sample cup. The cell number per millilitre was then determined with the Vi-CELL XR Cell viability analyser (Beckman Coulter Life Sciences, USA) that performs a live-dead cell staining and quantitation by trypan blue dye exclusion method. The advantage of automated compared to

manual cell counting is that every step from the staining to the cell counting is standardized and therefore more easy reproducible.

As there are several personalized machine settings possible (e.g. minimal/maximal diameter considered, etc.), they have to be specified for each cell type separately.

3.2.6 Cytotoxicity assay

To determine the blasticidin concentration, using as selection pressure after lentiviral transfection of keratinocytes, we performed a proliferation/cell viability assay. As the concentration for fibroblasts was already known from previous studies to be 5 µg/mL for the first two weeks of cultivation, six different concentrations (10 µg/mL, 7.5 µg/mL, 5 µg/mL, 3 µg/mL, 2 µg/ml and 0 µg/mL) were chosen to test on the keratinocytes. The cells were seeded in equal numbers and with around 90 % confluence into a six-well plate. KGM-2 supplemented with G418 and the various blasticidin concentrations was added to each well. For a period of eight days cells were observed daily under the light microscope to check cell viability, cytotoxicity and to gather the live/dead ratio. Images were captured every day. On day eight, the concentration at which 60–70 % confluence of the keratinocytes was still maintained, was chosen to be the concentration applying as selection pressure after lentiviral transduction.

3.2.7 Lentiviral transduction and cell line establishment

For cell line establishment HDF and NHEK/SVTERT 3-5 were infected with lentiviral particles containing one of three different genetic constructs, an empty vector, wild type *SNEV* and a mutated form of *SNEV* that cannot be phosphorylated by ATM. Therefore the serine at

position 149 has been mutated to alanine *SNEV*$^{(S149A)}$, using the QuickChange Multi Site-Directed Mutagenesis Kit (Agilent, USA). *SNEV* cDNA was amplified and ligated into the retroviral plasmid pLenti6. The lentiviral constructs were provided by the cooperating laboratory of Jansen-Duerr (University of Innsbruck).

Human dermal fibroblasts and epidermal human keratinocytes transfected with hTERT were seeded into one well of four 6-well plates with 50000 cells each and cultivated until they reach 50–60 % confluence. Respectively three plates of every cell line were used for transduction and one plate served as an un-transduced control, checking the selection reagent to work properly. 40 µL of each of the three different lentivirus were mixed with 1 mL culture media supplemented with 6 µg/mL polybren. The mixtures containing the viral particles were added to the HDF and NHEK/SVTERT in the 6-well plates and cells were incubated overnight. For the un-transduced control culture media containing 6 µg/mL polybren only was used. Thereafter, transfectants were selected using blasticidin (InvivoGen, USA) as a selective antibiotic. Only fibroblasts and keratinocytes carrying the blasticidin resistance gene encoded by the lentiviral construct survive the selection pressure. After one week, cells not carrying this gene are dead and selection is completed. The remaining cells were considered successfully transfected with either of the constructs. Depending on the construct inserted, the established cell lines were designated empty vector (neg. control vector), SNEV wt (wild type *SNEV*) and *SNEV*$^{(S149A)}$ (phosphorylation-mutated form of *SNEV*).

3.2.8 Proliferation assay

To assess the effect of *SNEV* on a cell population, a live-dead cell staining and quantitation by trypan blue dye exclusion method as described in 3.2.5 was performed.

Cells were seeded in equal numbers into six-well plates in triplicates and observed between four and six time points. On each time point cells were counted with the ViCELL-XR Cell

viability analyser and an average value and standard deviation of the triplicates were calculated.

3.2.9 (Indirect) Immunofluorescence staining

Immunofluorescence is a method based on antibody to antigen specificity. Every biomolecule for which a respective antibody exists can be targeted and visualized. There are two slightly different methods: Either the 1st antibody is directly labelled with a fluorochrome and can be detected under the microscope, as it was the case for the vimentin staining. Or – like for α-smooth muscle actin – there is a respective fluorescence labelled 2nd antibody that specifically binds the 1st antibody and which then can be visualized under the microscope.

First, cells were seeded into chamber slides (IBIDI 15 µl-slide 8-well, Germany) and cultivated 24–48 hours so that single cells are still easy discernable. The used volume for every step was 110 µL per chamber of the IBIDI slide. Cells were washed twice with PBS and fixed in 4 % paraformaldehyde (Roti® Histofix, Carl Roth, Germany) in PBS for 10 min at room temperature. Permeabilization was performed with 0.3 % Triton-X-100 in PBS + 10 % FCS for 10 min at room temperature. After an additional washing step, the cells were incubated for 1 h at 37°C with the first antibody diluted in 0.3 % Triton-X-100 + 10 % FCS. Following a washing step, if necessary cells were incubated with the appropriated secondary antibody diluted in PBS + 10 % FCS for another hour at 37 °C. Antibodies and the respective dilutions used are listed in Table 6. Cells were washed three times with PBS and the nuclei were counterstained with DAPI (500 ng/6 mL) for 10 min at room temperature. After a last washing step, the cells were covered with PBS and stored at 4 °C until microscopy was carried out.

For imaging and capturing the immunofluorescence staining, the Leica DMI6000B wide-field fluorescence microscope “LiveCell Setup” was used. It is composed of an EL600 fluorescent lamp and a CCD camera DFC360 (monochrome). The objectives HXC PL FLUOTAR

10x/0.30 Dry, WD: 11.0, DIC (11506505) and the HC PL APO CS 20x/0.070 ImmCorr: W-Gly-Oil, WD 0.26-0.17, DIC (11506323) were used.

Table 6. Antibodies and their respective secondary antibodies

1st Antibody	Dilution	2nd Antibody	Dilution
BD Pharmingen™ Alexa Fluor® 488 Mouse Anti-Human Vimentin	1:250	/	/
Sigma-Aldrich Monoclonal Anti-Actin, α-Smooth Muscle Clone 1A4	1:250	Jackson ImmunoResearch Alexa Fluor® 488 AffiniPure Donkey Anti-Mouse IgG (H+L)	1:500

3.2.10 Senescence associated β-galactosidase assay (SA-β-gal)

The standard method to visualize senescent cells is to stain for senescence-associated β-galactosidase activity at pH 6.0, characteristic for cells in an irreversible growth arrest.

The cultivated cells were washed with PBS and fixed 10 minutes in 2 % formaldehyde, 0.2 % glutaraldehyde in PBS. Subsequently, cells were washed twice with PBS and once with staining buffer (100 mM citrate buffer and 200 mM sodium phosphate, pH 6). Then, cells were incubated overnight at 37 °C with staining solution (400 mM sodium ferricyanide, 400 mM sodium ferrocyanide, 200 mM magnesium chloride, X-gal and staining buffer). On the following day, cells were examined under the light microscope, pictures were taken and senescent cells appearing blue were counted.

3.2.11 Stress induced premature senescence treatment (SIPS)

Replicative senescence refers to cells, which are irreversibly growth arrested but still are metabolically active. Senescence can be caused by several different factors including oxidative stress, dysfunctional telomeres and chromatin perturbations. For our purpose cells were chronically treated with hydrogen peroxide (H_2O_2) to induce a state of premature senescence.

Fibroblasts were seeded into 6-well plates and cultivated until they reached about 50–60 % confluence and single cells are still discernable. The experiment for every cell line was performed in duplicates and additionally one untreated well of each cell line served as a negative control. To reach the desired concentration of 60 mmol, 1.8 µL of the H_2O_2 stock solution (100 mmol) were diluted with 3 mL DMEM/Ham's media. Supernatant was removed from the cells and 1.5 mL of the H_2O_2 solution were added into each of two 6-wells. Then cells were incubated 1 hour at 37 °C in the incubator. Subsequently a medium change was performed and 2 mL fresh fibroblast medium was added to each 6-well. This step was also performed for the "control-well". The procedure was conducted for 10 days with an add-on recovery phase of additional 7 days, performing conventional medium change every 3rd day.

After recovery phase ended, one of the H_2O_2 treated 6-wells was stained for SA-ß-gal as well as the control well, while the other one was lysed in 0.5 mL trizol.

3.2.12 Ultraviolet A radiation treatment

UV radiation leads to DNA damage and can finally even initiate cell death. It is important to choose the type of radiation and the intensity according to requirements. Skin fibroblasts are embedded in the dermis, therefore we treated the cells with ultra violet (UV) A radiation. UVA has a wavelength of 315 to 400 nm and can penetrate into the dermis of the human skin.

Cells were seeded into 6-well plates and cultivated until they reached about 50-60% confluence and single cells are still discernable. The experiment was performed in duplicates plus one untreated well for every cell line, serving as a negative control. The control was covered with aluminium foil during the radiation. Supernatant was removed and 1 ml PBS was added into each well. On the on hand, PBS allows UVA to penetrate as it is colourless and on the other hand, it keeps the cells hydrated during radiation. The 6-well plate was placed into the radiating unit (Sellamed 1200, Sellas Medizinische Geräte GmbH, Germany) for 3 min and 40 sec with 10 J/cm^2 UVA. During the whole radiation process, the UVA chamber and the cells were cooled down using the F250 Recirculating Cooler (Julabo, Germany). Afterwards, PBS was replaced with 2 mL fresh medium and the cells were placed back into the incubator. The procedure was conducted for 7 days with an add-on recovery phase of additional 7 days, performing conventional media change every 3rd day.

After recovery phase ended one of the H_2O_2 treated 6-wells was stained for SA-ß-gal as well as the control well. The other well was used to prepare a trizol lysate.

3.2.13 Scratch assay

The scratch assay also known as wound healing assay mimics the process of wound healing in a monolayer cell culture. Cells are grown to 100 % confluence and with the tip of a pipette a scratch is made through the cell monolayer to simulate the wounding. Wound healing can be influenced by several factors and we wanted to show the effect of *SNEV* overexpression on wound healing. For the experiments keratinocytes served as the monolayer cell culture that was wounded because the epidermis and the *Stratum corneum* of human skin are composed of these cells. After wounding cells were cultivated for another 24 hours and images of the whole scratch were taken every three hours, to determine the extend of wound closure.

NHEK/SVTERT were cultivated in 12-well plates using KGM-2 media supplemented with 50 µg/mL G418. At the moment they reached 90-100 % confluence, supernatant was

discarded and a scratch of around 5 mm length was made with a 200 µL pipette tip (Greiner Bio-one, Austria). After a washing step with PBS, 1 mL KGM-2 media without G418 was added into each 12-well. Subsequently images of every scratch were taken with a light microscope (Leica DMIL LED, Germany). At this step it was important to capture the whole scratch very precise without any overlaps and/or gaps, so that the total area of each "wound" could be calculated from the sum of all images. Pictures were taken every 3 hours at least for 9 hours. Between imaging the plates were incubated with 7 % CO_2 at 37 °C.

To investigate the influence of secretion factors of *SNEV* overexpressing fibroblasts on keratinocytes in wound healing, conditioned media from transduced HDFs was added to NHEKs. Conditioned medium was produced by cultivating *SNEV* overexpressing human dermal fibroblasts until they reached approximately 70 % confluence in a T25 roux flask. Then a medium change with KGM-2, which was used as growth medium for NHEKs, was carried out and the cells were cultivated for additionally 48 h. Subsequently, the conditioned media was transferred from the roux flasks into 15 mL Falcon tubes and spun down for 10 min at 500 x g to get rid of cell debris. In parallel, normal human keratinocytes were cultivated in 12-well plates until 90–100 % confluence, then supernatant was discarded and a scratch of around 5 mm length was made with a 200 µL pipette tip. After a washing step with PBS, 1 mL of the prepared conditioned media was added into each well. All following steps were exactly performed as mentioned above.

Analysis of the images to determine the total scratch area was conducted using the software ImageJ. All pictures needed to be converted to a pixel size of 2592 x 1944 pixels, allowing comparison of different scratches and/or different time points with each other. The extend of wound healing was ascertained as a percentage of the initial scratch area.

3.2.14 Collagen contraction assay

This assay enables the measurement of the contraction capability of cells embedded in a collagen gel. It can give indication how different cell types influence wound healing with respect to wound contraction.

Preparation of collagen for use in collagen gels:

The collagen solution has to be prepared fresh before every new experiment. Thereto 3 mL collagen G (4 mg/mL, Merck Biochrome GmbH, Germany) and 1 mL precooled acetic acid solution (1%) are mixed well to obtain a collagen concentration of 3 mg/mL and stored at 4 °C until used. The acetic acid creates an acidic environment, necessary to keep the collagen soluble.

Cultured fibroblasts were harvested by trypsinization and the cell number was determined as described in 3.2.5.. The remaining cell suspension was centrifuged for 5 min at 170 x g. The supernatant was discarded and the cell pellet re-suspended in the appropriate volume of DMEM/Ham's F12 (1:1) supplemented with 10 % FCS and 4 mM L-glutamine to reach a cell concentration of 1.5 x 10^5 cells/mL. 1.6 mL of the cell suspension was transferred into a fresh 15 mL Falcon tube. After adding 0.8 mL collagen solution (3 mg/mL) to the cells, the colour changed from light rose to yellow, indicating an acidic state. After mixing properly, 1M NaOH was added until the colour turned pink again (approximately 30 µl). The colour change indicates the neutralization of the collagen-cell solution, necessary for the cells to survive. 500 µL of the obtained cell gel mixture were pipetted carefully into a 24-well plate, avoiding formation of air bubbles. All experiments were carried out in quadruplicates in 24-wells. The plates were incubated for 2–4 hours at 37 °C until the gel was solidified. Subsequently, 600 µL Optimem (Thermo Fisher, USA) were added to each well and the gels were gently dissociated from the well by running a 200 µL pipette tip along the edges, taking care not to shear the gels. To check if the gels are completely detached, the plate was carefully swirled. During the following 9 h, pictures were taken every three hours. To make the images comparable with each other and between the different time points, the angle and distance from the plate to the camera were kept constant through the experiment.

To determine the gel area, the images were analysed with the software ImageJ making sure all had the same size of 2448 x 3264 pixels. The extend of contraction was ascertained as a percentage of the initial gel size.

3.3 RNA analysis

3.3.1 RNA isolation using TRI Reagent®

Purified, isolated RNA is prone to degradation by RNases. Therefore, it is important to work very carefully, always using RNase free water and RNase inhibitors to avoid any contamination of the RNA and to achieve sufficient yield and purity.

TRI Reagent® (Sigma-Aldrich, USA) is a mixture of guanidine thiocyanate and phenol in a monophase solution. It is used for simultaneous isolation of RNA, DNA and protein by a single-step liquid phase separation.

For preparation of trizol lysates and subsequent RNA isolation, fibroblasts were cultured until they reached approximately 90–100 % confluence, and keratinocytes until 70 % confluence in 6-well plates. After removing growth medium and washing cells once with PBS, 0.5 mL TRI Reagent® were added to each well, cells were detached by pipetting up and down and the lysate was transferred into RNase free microcentrifugation tubes (Sarsted, Germany). The trizol lysates were either stored at -80 °C or used directly for RNA purification.

3.3.2 RNA purification

RNA was isolated from trizol lysates using an organic extraction method. The trizol lysates were homogenized with chloroform and after centrifugation the mixture was separated into three phases: an organic phase (containing protein), an interphase (containing DNA) and a colourless upper aqueous phase (containing RNA). The upper aqueous phase was recovered and RNA collected by alcohol precipitation and rehydration. Purity and amount of isolated RNA are crucial to run subsequent molecular techniques such as quantitative PCR.

100 µL chloroform (Sigma-Aldrich, USA) was added to each 500 µL tryzol lysate, mixed by vortexing and incubated for 3 min at room temperature. After a centrifugation step of 15 min at 1200 x g and 4 °C, 200µl of the upper aqueous phase containing the RNA were carefully transferred into a fresh microcentrifugation tube (Sigma-Aldrich, USA), avoiding contamination with the other phases. Next, 250 µL isopropanol (Merck, USA) and 1 µL glycoblue (Thermo Fisher, USA) were mixed with each RNA sample and incubated for 10 min at room temperature. Glycoblue served as a nucleic acid coprecipitant, increasing visibility of the pellet. Another centrifugation step for 10 min at 1200 x g and 4 °C resulted in a RNA pellet at the bottom of the microcentrifugation tube. Supernatant was removed and the pellet was washed by adding 500 µL 70 % ethanol (Merck, USA) and centrifuging 5 min at 7600 x g and 4°C. Again, supernatant was completely removed and the pellet air-dried for 10–15 min in the hood. Finally, the pellet was dissolved by adding 20 µL RNAse-free water and incubation in the Thermomixer comfort (Eppendorf, Germany) at 55–66 °C for 10 min without shaking. The RNA samples were stored for at least 1 h at -20 °C before quantification.

3.3.3 RNA quantification

The RNA concentration was determined to evaluate if the RNA isolation and purification was successful and yielded high quality samples. For many further experiments it is necessary to use an exact amount of RNA.

Quantification of the RNA concentration was performed using Nanodrop One UV-Vis Spectrophotometer (Thermo Scientific, USA). Since DNA has the same absorbance as RNA at 260 nm it is important to avoid contamination with DNA during purification. Furthermore the device determines the absorbance at 230 nm and 280 nm to asses the degree of contamination with organic solvents and/or proteins. The ratio of 260 nm/230 nm should exceed 2.00 for successful subsequent experiments including enzymatic reactions. TRI Reagent® residues are reflected by this ratio, which inhibit reactions like reverse transcriptase activity. The 260 nm/280 nm absorbance ratio is used as a measurement for RNA purity. A ratio of at least 1.80 is considered acceptable.

3.3.4 Complementary DNA synthesis

Complementary DNA (cDNA) is single stranded deoxyribonucleic acid synthesized from a single stranded RNA template via reverse transcription. cDNA is compared to DNA more stable and has a longer half-life, a big advantage when storing samples. Reverse transcription is a very powerful tool since it allows you to circumvent the dogma of molecular biology, which prescribes the hierarchy from DNA to RNA to protein.

For reverse transcription, the High-Capacity cDNA Reverse Transcription Kit (Applied Biosystems™, USA) containing MultiScribe® Reverse Transcriptase (50 U/µL), 25X dNTP Mix (100 mM), 10X RT Random Primers and 10X RT Buffer was used. Additionally, RNase free water and the RNase inhibitor Recombinant RNasin® (Promega, USA) was employed.

500 ng RNA in a volume adjusted to 10 µL were pipetted into a PCR-tube. Then 10 µL master mix were added. The composition of the mastermix is listed in Table 7. After a short spin down the tubes were placed into the T3 Thermocycler (Biometra, Germany) and the PCR program (Table 8) could be started.

Table 7. Mastermix composition for cDNA synthesis using the High-Capacity cDNA Reverse Transcription Kit

Total volume per reaction	20 µL
Number of reactions	1
Volume template	10 µL
10X RT Buffer	2 µL
25X dNTP Mix (100 mM)	0.8 µL
10X RT Random Primers	2 µL
RNasin®	1 µL
MultiScribe® Reverse Transcriptase	1 µL
RNase free water	3.2 µL

Table 8. Cycling parameters for cDNA synthesis

Temperature (°C)	**Time**
25	10 min
37	120 min
85	5 min
15	pause

3.3.5 Real–time quantitative polymerase chain reaction (qPCR)

Real–time quantitative PCR is known as the gold standard for gene expression analysis, and is commonly used to validate results obtained from high-throughput technologies such as microarray and next-generation sequencing. It was the standard method for quantification of messenger RNA (mRNA) expression in this thesis. Within conventional PCR reactions there is a lot of variability due to polymerase inhibitors or reagent limitation, just to mention a few. This variability can be minimized by the quantitation of accumulating PCR products in the exponential phase as it is done by qPCR(Raeymaekers 2000).

SYBR Green is a nonsequence-specific, ds-DNA-intercalating agent, meaning detectable fluoresce intensity depends on the amount of ds-DNA present in the reaction(Morrison et al. 1998). As it is susceptible to generate false positive fluorescent signals due to nonspecific binding to any ds-DNA, including for example primer-dimers or nonspecific PCR products(Ririe et al. 1997), we decided to use EvaGreen to perform qPCR. EvaGreen has a much lower tendency to generate fluorescence signal due to intercalation with unspecific amplificates. Furthermore, it exhibits a sharper and stronger DNA melt peak(Mao et al. 2007).

Rotor-Gene Q (Quiagen, Netherlands) and the compatible Q Rex Software (Quiagen, Netherlands) were used to conduct and analyse qPCR. In order to quantify the specific PCR product for the used qPCR primers, the detected fluorescence signal was compared to its respective standard curve. The calibration curve was calculated using the Q Rex Software.

Standard preparation:

The standards were prepared using cDNA as a template and genomic DNA as a negative control, as the used primers should span an intron and thereby produce no suitable PCR product with genomic DNA. cDNA and DNA should preferably be from the same cell type mRNA levels want to be determined. The first step was a PCR reaction with GoTaq G2 polymerase and green reaction buffer as listed in Table 9 with the respective thermocylcer program (Table 10).

Table 9. GoTaq G2 PCR Mastermix

Total volume per reaction	50 µl
Number of reactions	1 µl
Volume template	1 µl
5x GoTaq green reaction buffer	10 µl
dNTP Mix (10 mM)	1 µl
GoTaq G2 DNA Polymerase	0.25 µl
Nuclease free water (NFW)	34.75 µl

Table 10. Cycling parameters for qPCR standards

Steps	Temperature (°C)	Time
1	95	5 min
2	95	30 sec
3	55	30 sec
4	72	20 sec
5	Repeat steps 2-4 39 times	
6	72	5 min

After the PCR, the samples and a 100 base pair ladder were loaded on a 2 % agarose gel and gel electrophoresis was run at 130 V for approximately 1 hour. Subsequently, the lengths of the PCR products were compared with the calculated lengths and if consistent the bands were cut and DNA was purified with the FavorPrep GEL/PCR Purification MiniKit (Favorgen Biotech Corp., TWN). After calculation of the copy number a qPCR standard solution with nuclease free water (NFW) containing 10^9 copies/uL was prepared and stored at -20 °C until used.

Quantitative PCR:

For quantification of mRNA every qPCR run needs to include the standards of the mRNA of interest in the range of 10^8–10^3 copies. Standards are measured in duplicates, samples in quadruplicates. For qPCR 9 µL mastermix were pipetted into PCR tubes (PCR 0.1 mL 4 Tube & 4 Cap Strips Biozym, Austria) and 1 µL template was added into each. Mastermix was prepared as depict in Table 11. Reagents and samples are kept on cool blocks throughout the whole procedure.

Table 11. Mastermix composition for qPCR

Total volume per reaction	10 µL
Number of reactions	1
Volume template	1 µL
Primer sense	0.25 µL
Primer antisense	0.25 µL
Reaction buffer	2 µL
RNase free water	6.5 µL

The caps needed to be closed properly before the tubes were equilibrate loaded into the Rotor Gene Q cycler. The exact cycle steps are listed in Table 12.

Table 12. Cycle steps of the qPCR program

Step	**Temperature (°C)**	**Time**	**Cycles**
Polymerase activation	95	15 min	1
Denaturation	95	15 sec	45
Primer annealing	50–55	30 sec	
Extension	72	15 sec	
Melting curve	100	0	1

To quantify expression levels of genes of interest standard curves reaching from 10^8 to 10^3 copies were made. Standard values were gathered together with the samples in the same run. Subsequently expression levels were normalized to an appropriate housekeeping gene determined in advance. A gene, which is essential for basic cell maintenance and therefore, is expressed in a constant level in different conditions, is termed a housekeeper(Eisenberg and Levanon 2013). In our experimental set up *glyceraldehyde-3-phophate dehydrogenase (GAPDH)* seemed to be a suitable housekeeping gene. It is important to choose the housekeeper carefully since its expression level influences the accuracy of the results.

3.4 Statistics

An unpaired t-test was the hypothesis test performed to evaluate the statistical significance. The *P*-value another terminology of Type I error rate, reflects the probability of making the error of stating that there is a difference between two sample groups when there is no difference. Tests with a type 1 error probability < 0.05 were marked as * (significant), < 0.01 as ** (very significant), < 0.001 as *** (highly significant) < 0.0001 as **** (extremely significant). The error bars represent ± SD.

4 Results

4.1 Characterization of the function of *SNEV* in human dermal fibroblasts

4.1.1 Generation of stable *SNEV* overexpressing human dermal fibroblasts

To study the role of *SNEV* in skin cells, it was a prerequisite to generate stable fibroblast cell lines overexpressing *SNEV*. Cells were transfected with lentiviral particles carrying one of three different constructs, either a negative control vector, wild type *SNEV* or a phosphorylation mutated form of *SNEV*. According to that, the resulting cell lines were named empty vector (negative control vector), *SNEV* wt (wild type *SNEV*) and $SNEV^{S149A}$ (phosphorylation-mutated form of *SNEV*). Transfectants were selected using 5 ug/mL balsticidin. Population doublings (PD) post transduction (pT) start to be counted with the first passage after selection was completed. The effect of phosphorylation insufficient $SNEV^{S149A}$ was analysed additionally to *SNEV* overexpression as it was known from previous experiments that the phosphorylation of *SNEV* is important for growth regulation and stress repair. Furthermore, a knock out/knock down of *SNEV* is not possible and the phosphorylation-insufficient $SNEV^{S149A}$ represents a good alternative.

In fibroblast cell lines derived from three different donors (HDF85, HDF76, HDF161) a successful *SNEV* overexpression by lentiviral transduction was achieved. Overexpression was verified by qPCR. As indicated in Figure 6, the overexpression of wild type *SNEV* in fibroblasts reached from 2-fold in HDF85 to nearly 7-fold in HDF76. The values were normalized to HDF76 empty vector. As most of the data from our previous studies were obtained in fibroblast donor cell line HDF76, we conducted our following experiments with these cells and tried to verify the results in other donors.

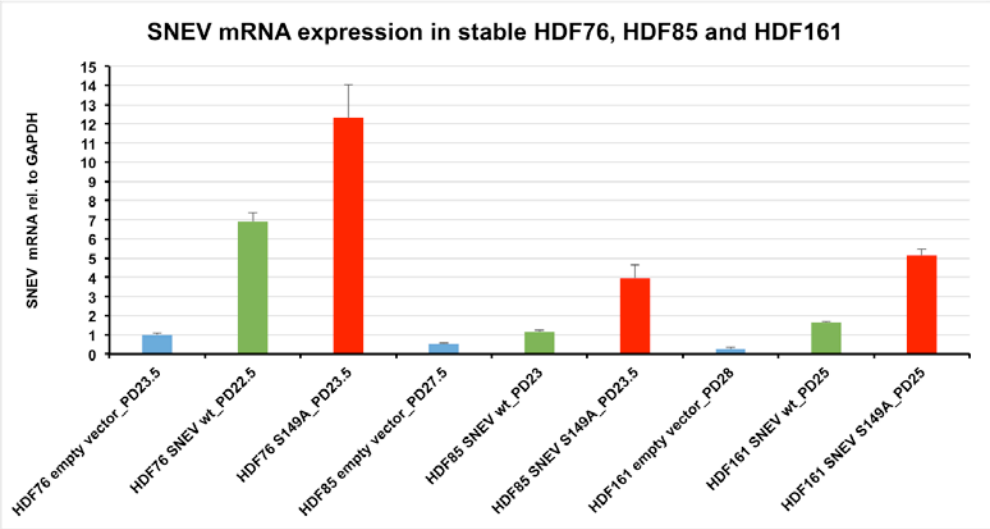

Figure 6: Conformation of successful *SNEV* overexpression in fibroblasts. Respective empty vector, *SNEV* wt and *SNEV*^{S149A} mRNA expression levels in human diploid fibroblasts

4.1.2 *SNEV* induces a papillary/juvenile morphology in human dermal fibroblasts

4.1.2.1 Observed morphological changes by light microscopy

As the lentiviral transduction was successful we further cultivated the fibroblasts. Interestingly, we observed significant morphological difference between the cell lines empty vector, *SNEV* wt and *SNEV*$^{(S149A)}$. Whereas fibroblasts transduced with empty vector or phosphorylation insufficient *SNEV*^{S149A} showed a more reticular morphology from the very beginning on and developed a characteristic senescent phenotype, *SNEV* wt cells appeared more papillary and juvenile throughout the whole culture period of 5 months (Fig. 7). Typically for a reticular phenotype is a flat, spread out cell, sometimes dotted with a lot of vacuoles. In contrast, a papillary morphology is characterized by long, slim, spindle-like cells that grow denser. These two morphological phenotypes are designated to the two different types of fibroblasts in the human dermis (papillary and reticular fibroblasts), which show other characteristics and functions.

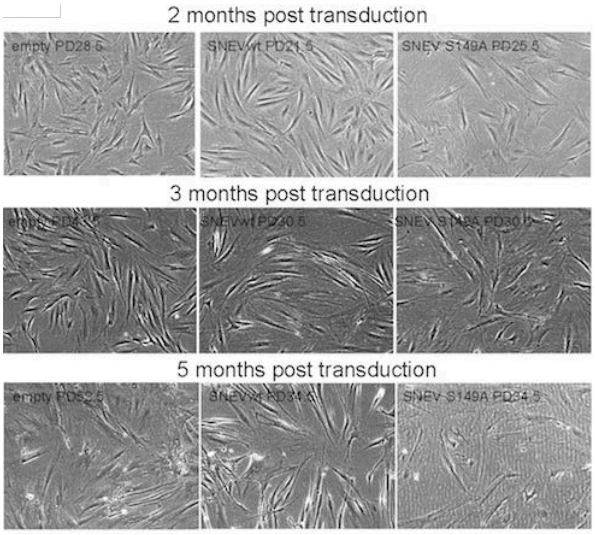

Figure 7: *SNEV* overexpressing fibroblasts are characterized by a more papillary/juvenile morphology. Light microscopy pictures after 2, 3 and 5 months of culture.

4.1.2.2 Quantification of morphological changes

To quantify morphological changes observed by light microscopy, we performed an immunofluorescence staining using an anti-vimentin antibody coupled with Alexa Fluor® 488 and counterstained the nuclei with DAPI. This antibody specifically binds to vimentin, one of the intermediate filaments the cytoskeleton is composed of, depicting the cell shape and area of the fibroblasts. With the cell image analysis software CellProfiler we quantified compactness, eccentricity, major and minor axis length, perimeter and spreading area of the cells. The software automatically recognizes the area of each cell and calculates the respective parameters reflecting fibroblast morphology. In this case compactness was defined as the variance of the radial distribution normalized by the area, meaning the higher the value the more elongated the cell. The eccentricity is the ratio of the distance between the foci of the ellipse and its major axis length. The value can reach from 0 to 1, meaning the lower the value the more circular the cell.

The morphological phenotypes observed by light microscopy could be confirmed by immunofluorescence staining. Evaluation of the fluorescence signal displayed a more reticular morphology considering empty vector as well as *SNEV*$^{(S149A)}$ (Fig. 8). *SNEV* wild type overexpressing cells were assigned to cells with a more papillary and juvenile silhouette as it can be seen in Figure 8A (middle panel). They are long, spindle-like cells with a bright fluorescent signal.

To quantify the fluorescence intensity of the fibroblasts we used the software ImageJ. Each cell area was individually framed and measured. The quantification of the fluorescence intensity revealed a value of 91707 arbitrary units for *SNEV* wt, which was significantly higher compared to empty vector control fibroblasts (Fig. 8B). The highest value was determined for cells transduced with the phosphorylation-mutated form of *SNEV*^{S149A} with 321136 arbitrary units.

As we then had a closer look on the immunofluorescence staining we were able to define six parameters that perfectly reflect the cellular shape of the different recombinant fibroblast cell lines. As depicted in figure 8C compactness, eccentricity and major axis length were significantly more pronounced in wild type *SNEV* overexpressing fibroblasts compared to empty vector. Whereas, the parameters minor axis length, cell perimeter and spreading area were significantly less distinct compared to empty vector, which accounts for a longer and more spindle like morphology of wild type *SNEV* overexpressing fibroblasts. Cells transduced with phosphorylation incompetent *SNEV*$^{(S149A)}$ were similar to empty vector control fibroblasts, showing lower values for compactness and eccentricity, but higher values for minor axis length, cell perimeter and spreading area compared to *SNEV* wt.

In summary these findings indicate, that only the overexpression of wild type *SNEV*, but not its phosphorylation incompetent form induces a morphological change to a more papillary/juvenile fibroblast phenotype.

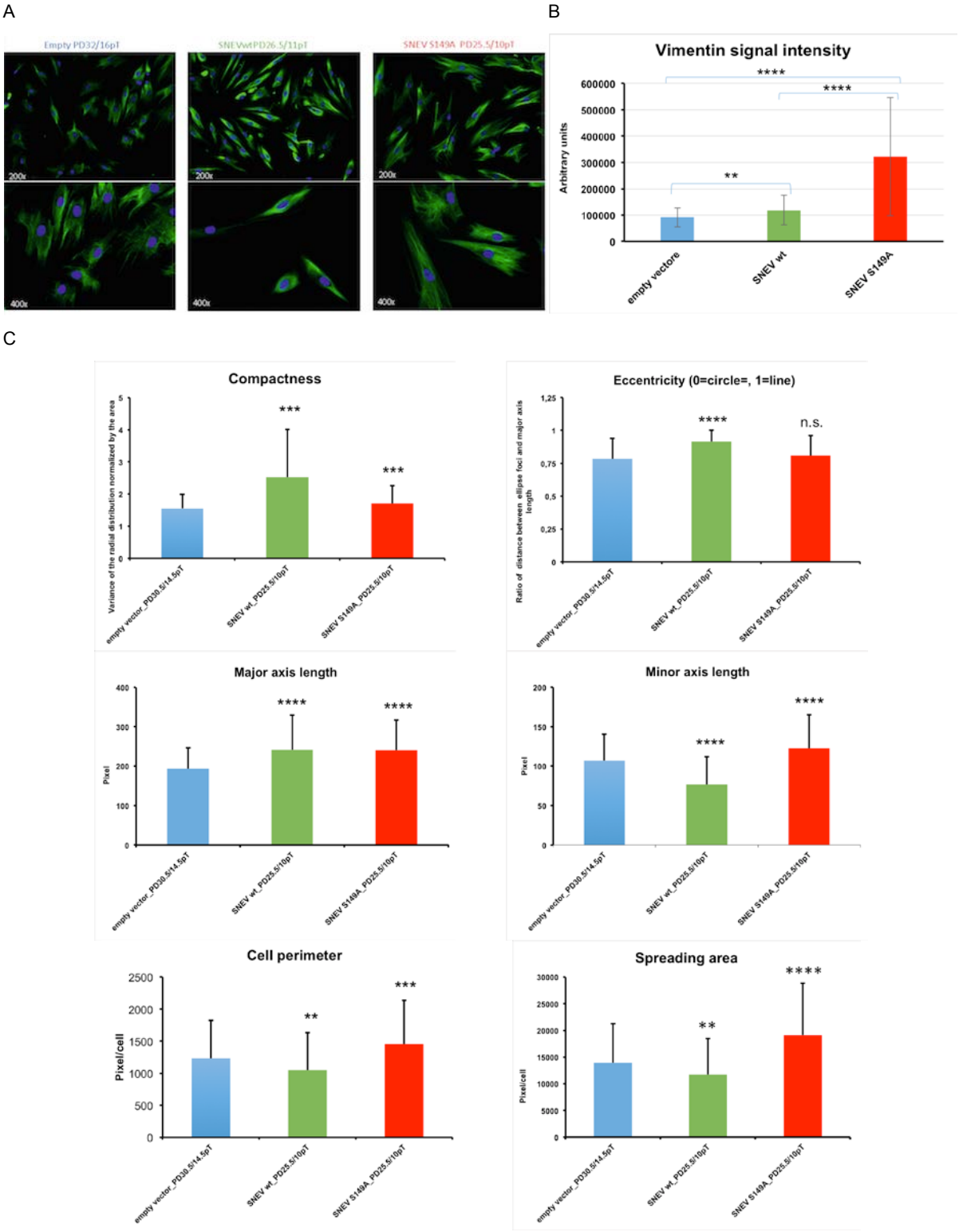

Figure 8: *SNEV* induces a papillary/juvenile morphology in fibroblasts. (A) Anti-vimentin fluorescence staining on fibroblasts seeded on coverslips. Nuclei are counterstained with DAPI. Magnification upper panel x 20, lower one x 40. (B) Respective calculation of the anti-vimentin fluorescence signal using ImageJ. (C) Analysis of parameters reflecting cell shape and morphology using the software Cell Profiler.

4.1.2.3 qPCR expression of papillary and reticular marker genes

In order to detect mRNA expression changes possibly underlying morphological changes, we also performed real time quantitative PCR. NTN1 and PDPN served as papillary and TGM-2 as well as PPP1R14A as reticular marker genes. Those markers have previously been identified by gene expression screenings of papillary versus reticular fibroblasts(Janson et al. 2012). Indeed in *SNEV* wt the papillary marker genes were higher expressed compared to empty vector and *SNEV*$^{(S149A)}$ (Fig. 9 upper panel). Expression of the reticular markers TGM-2 and PPP1R14A was higher in empty vector and *SNEV*$^{(S149A)}$ cells compared to fibroblasts overexpressing wild type *SNEV*.

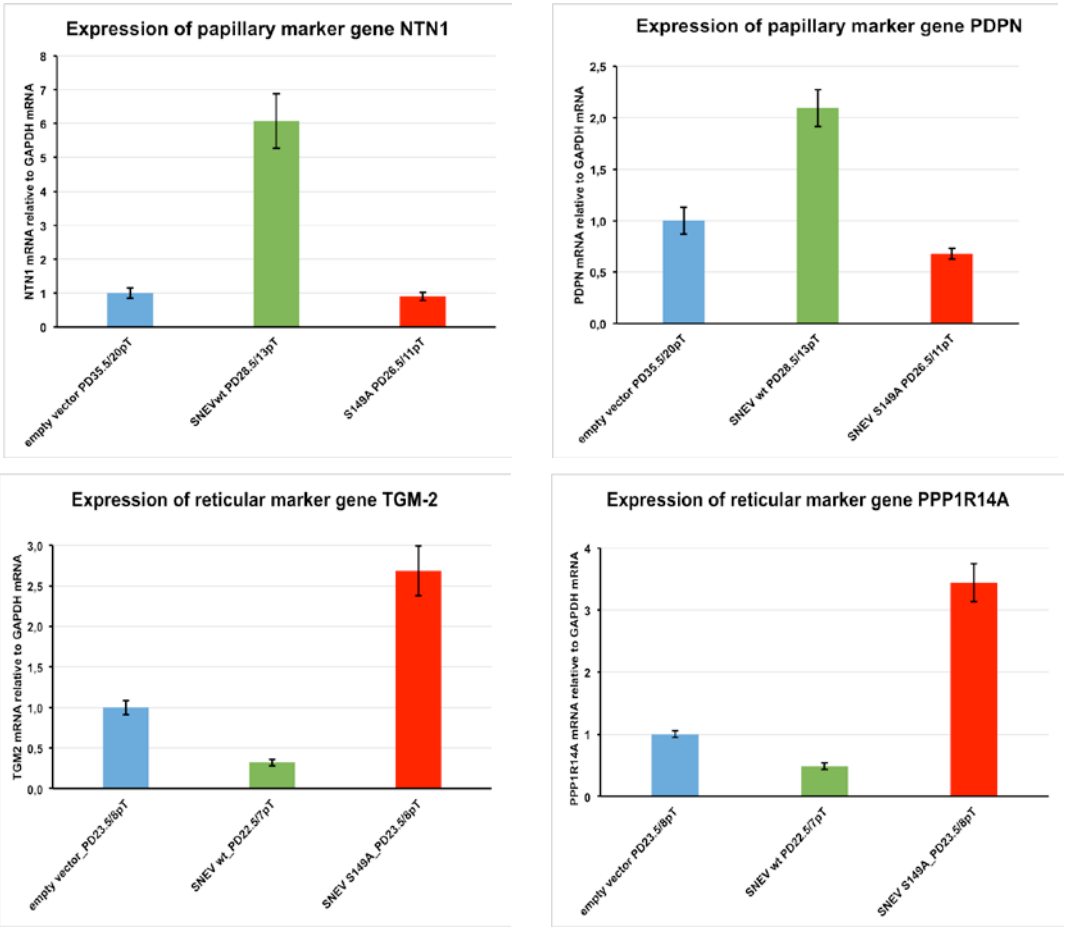

Figure 9: Expression of papillary and reticular marker genes. The respective qPCR results for papillary and reticular marker genes are depicted. Every sample was analysed in quadruplicates. Values were normalized to empty vector.

4.1.3 *SNEV* overexpression reduces fibroblast growth potential

We cultivated the recombinant fibroblast cell lines for more than 5 months and created a growth curve on the basis of population doublings post transduction. As shown in Figure 10A, SNEV wt underwent less population doublings during time of culture compared to empty vector. To asses if this is an effect of reduced growth or enhanced susceptibility to senescence we conducted a proliferation assay over 16 days. Wild type *SNEV* overexpressing fibroblasts showed reduced growth potential throughout the whole culture period compared to empty vector control cells (Fig.10B). The greatest difference could be observed at day 10 with 0.135 x 10^6 cell counts more in cells transduced with empty vector. Moreover, in long and short-term cultivation *SNEV*$^{(S149A)}$ displayed most decreased growth potential. These fibroblasts underwent only 17 PDs after 192 days in culture and 0.200 x 10^6 cells were counted less after 16 days in culture compared to empty vector.

A B

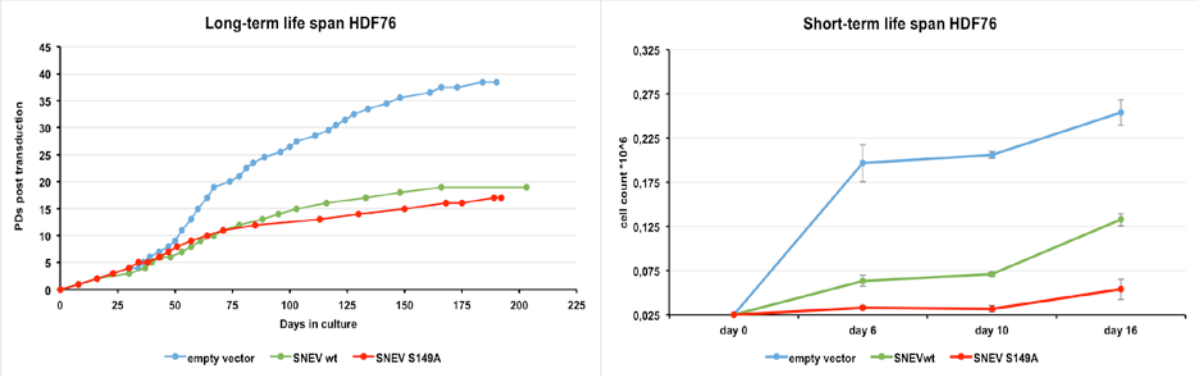

Figure 10: Reduced growth in *SNEV* overexpressing fibroblasts Life spans of fibroblasts determined in long (A) and short (B) term cultivation.

4.1.4 *SNEV* overexpressing fibroblasts modulate wound healing

4.1.4.1 *SNEV* overexpressing fibroblasts enhance keratinocyte migration

Scratch assays are used to simulate wound healing. Therefore, as described previously a scratch was made on a monolayer cell culture and cell migration into the wounded area was observed. Figure 11A illustrates the change of the scratch area from time point 0 (light grey) to time point 9 (black). As we wanted to asses if *SNEV* overexpressing fibroblasts have an influence on keratinocyte migration into the wounded area, we cultivated the NHEK after wounding with conditioned media of the transduced fibroblasts. In all three experiments we performed, we observed the same results: Keratinocytes cultivated with media from *SNEV* wt HDF76 migrated faster to the wounded area then those kept in conditioned media from *SNEV*$^{(S149A)}$ and empty vector fibroblasts (Fig. 11B). The slowest wound closure was observed for keratinocytes cultivated with media from HDF76 empty vector. Thus we concluded that *SNEV* overexpression in fibroblasts enhances keratinocyte migration, and this is dependent on phosphorylation by ATM.

A

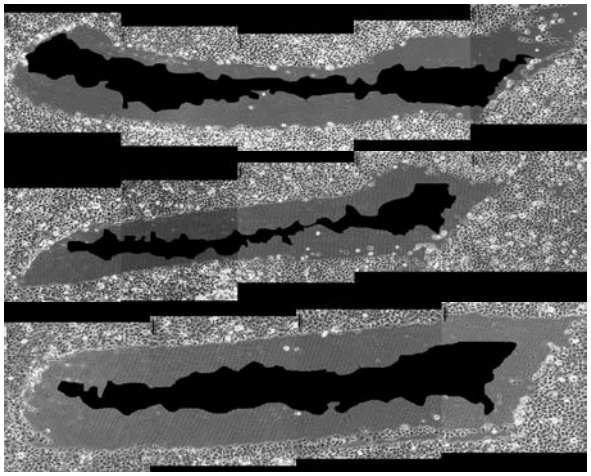

B

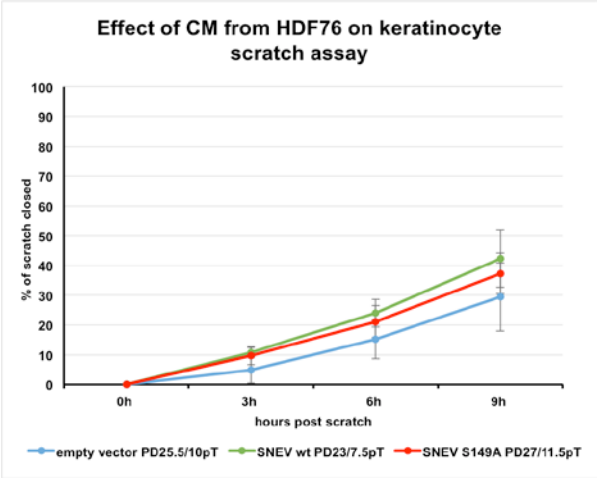

Figure 11: *SNEV* overexpressing fibroblasts modulate keratinocyte migration. (A+B) Wound healing assay using keratinocytes grown in conditioned media from *SNEV* overexpressing and control fibroblasts.

4.1.4.2 *SNEV* alters fibroblast contractility

Wound healing capacity is also associated with contractility; we assessed a possible effect of *SNEV* on wound contraction by two independent methods.

First, we quantified expression of α-SMA, a protein present in skeleton muscles belonging to the actin family and involved in the contractile apparatus, cell mobility and wound contraction. The fluorescence signal was significantly higher in fibroblasts overexpressing wild type *SNEV* compared with empty vector control cells. The highest α-SMA expression was observed in *SNEV*$^{(S149A)}$ HDF76 (Fig. 12A+B). Fluorescence intensity was quantified as described previous, using the software ImageJ.

In addition to gather information on a role of *SNEV* in wound healing/ contraction, we performed collagen contraction assays. The assay is used to asses the ability of cells to contract a collagen matrix. The results didn't significantly differ between empty vector and SNEV wt (Fig. 12C+D). *SNEV* seems to facilitate stronger contractility at early time points, but after 12 hours no significant differences were obtained between *SNEV* wt and empty vector cells. Nevertheless, phosphorylation incompetent *SNEV*$^{(S149A)}$ clearly showed reduced contractility of the fibroblasts. We noticed high technical variations and a bad reproducibility between the different conducted collagen contraction assays. The assay needs to be repeated, and a method serving reproducible results needs to be established in future investigations.

There is evidence that *SNEV* modulates the role of fibroblasts and subsequently via their secretion factors the role of keratinocytes, but further research is necessary.

A

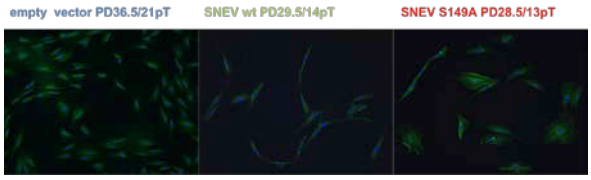

B

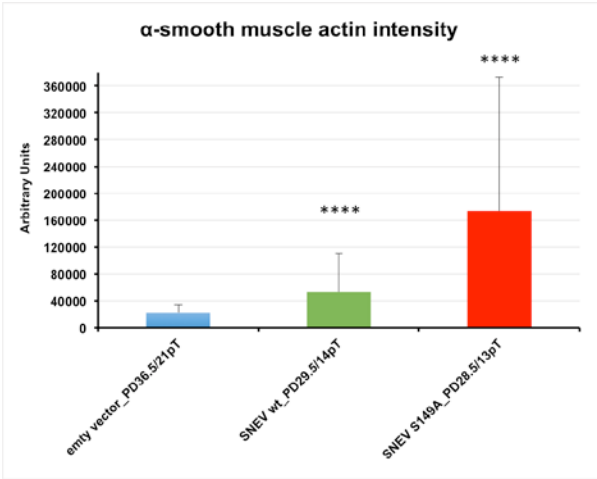

C

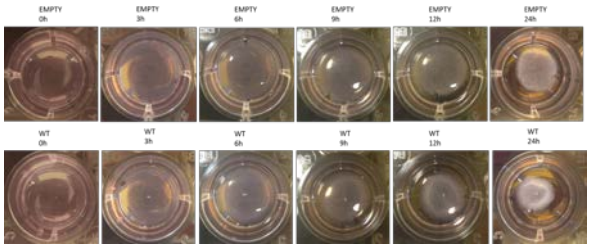

D

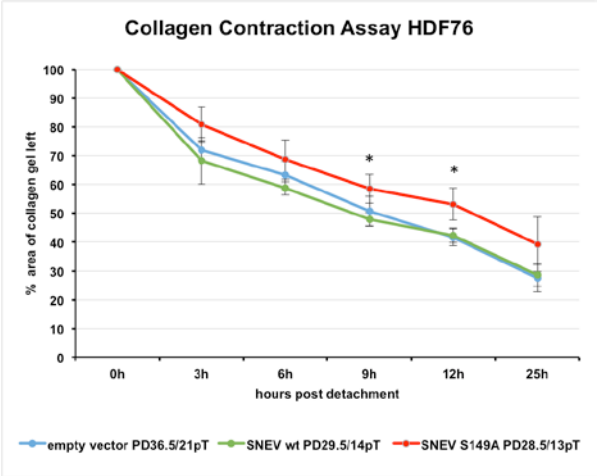

Figure 12: *SNEV* modulates contractility of human dermal fibroblasts. (A) Immunofluorescence staining of fibroblasts with anti α-SMA. Nuclei were counterstained with DAPI. (B) Respective calculation of the α-SMA fluorescence signal using the software ImageJ. (C+D) Collagen contraction assay. Samples were analysed in quadruplicates.

4.1.5 Influence of *SNEV* in cellular senescence of human dermal fibroblasts

4.1.5.1 Basal SA-β-galactosidase expression of recombinant fibroblasts

To further investigate if *SNEV* plays a role in premature ageing, a staining for the widely accepted senescence marker SA-β-galactosidase was performed. The results were not as expected from previous experiments in HUVECs. In young recombinant fibroblast cell lines *SNEV* wt showed a slightly, however not significant, higher SA-β-gal expression level compared to empty vector (Fig. 13A). In higher PDs there was no significant difference in SA-β-gal expression observed between empty vector, *SNEV* wt and *SNEV*$^{(S149A)}$.

A

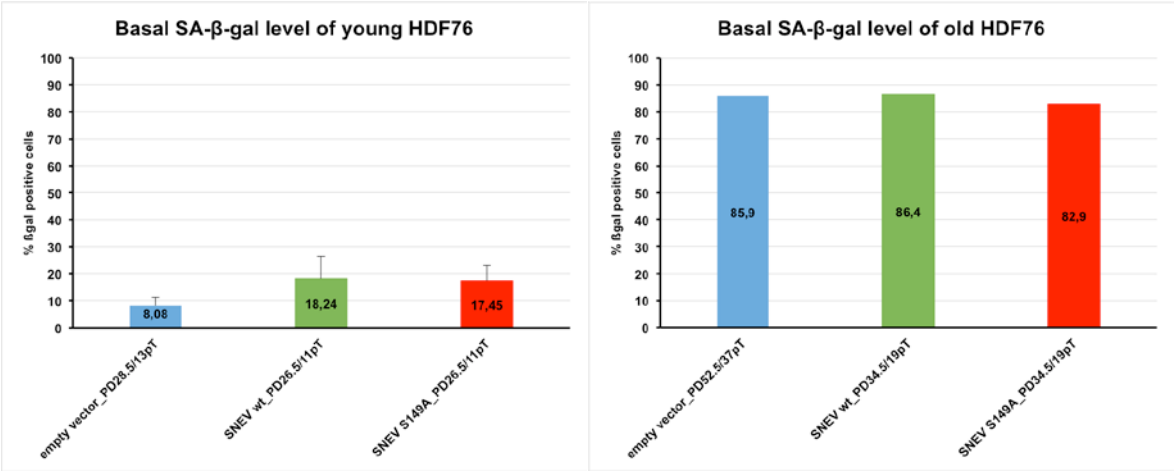

B

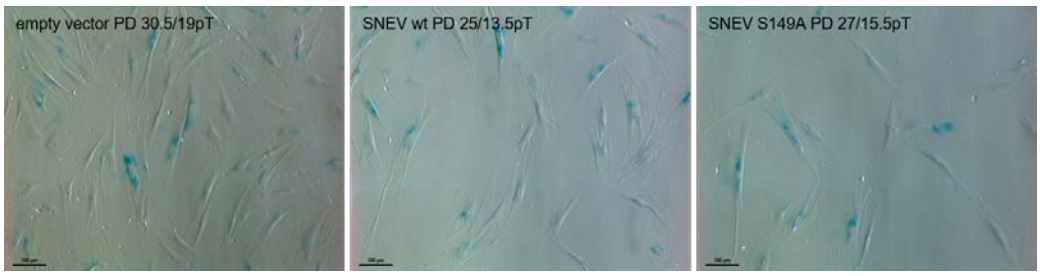

Figure 13: Effect of *SNEV* on basal SA-β-gal expression level. (A+B) Basal SA-β-gal expression levels in young and old recombinant fibroblast cell lines. Young HDF76 were analysed in triplicates. (B) SA-β-gal staining of recombinant fibroblast cell lines. Scale bars indicate 100 µm.

4.1.5.2 Role of *SNEV* in stress-induced senescence

Additionally, SA-β-gal expression levels were determined after chronic SIPS and UVA treatment, which are known to induce DNA damage. After SIPS treatment there was the trend that less *SNEV* overexpressing fibroblasts stained positive for SA-β-galactosidase compared to empty vector control cells (Fig. 14A). As depicted in Figure 14B, this trend could also be seen after chronic UVA treatment even not in the same extent. There was also no clear difference between *SNEV*$^{(S149A)}$ and empty vector control cells after SIPS and UVA treatment.

A

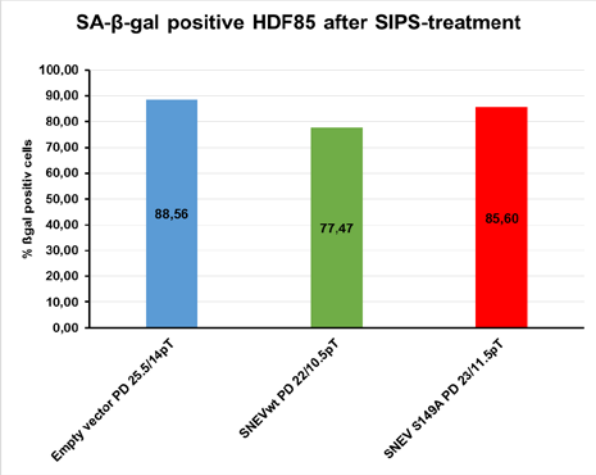

B

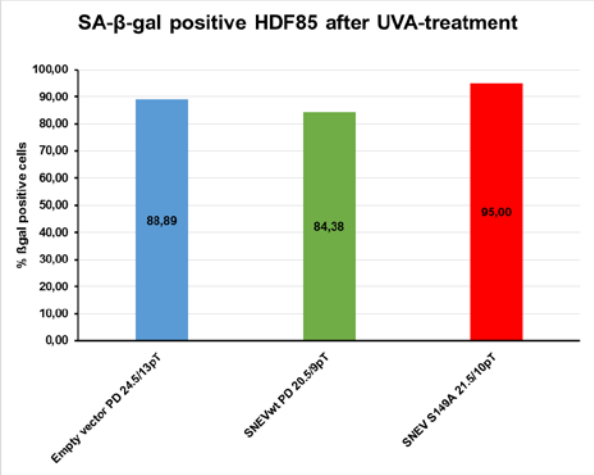

Figure 14: Effect of *SNEV* in stress-induced senescence. SA-β-gal expression levels in recombinant donor fibroblast cell lines after chronic SIPS (A) and UVA (B) treatment.

4.2 Characterization of the function of *SNEV* in normal human epidermal keratinocytes

4.2.1 Generation of stable *SNEV* overexpressing normal human epidermal keratinocytes

We wanted to investigate the role of *SNEV* in skin aging and skin function. For this reason we overexpressed *SNEV* not only in fibroblasts but also in keratinocytes. Successful *SNEV* overexpression was achieved in the immortalized keratinocyte cell line NEHK/SVTERT 3-5, by lentiviral transduction (Fig.15). We generated three stable NHEK/SVTERT cell lines overexpressing either wild type *SNEV*, the phosphorylation mutated form *SNEV*$^{(S149A)}$ or an empty vector. Accordingly, the cell lines were termed empty vector, NHEK *SNEV* wt and NHEK *SNEV*$^{(S149A)}$.

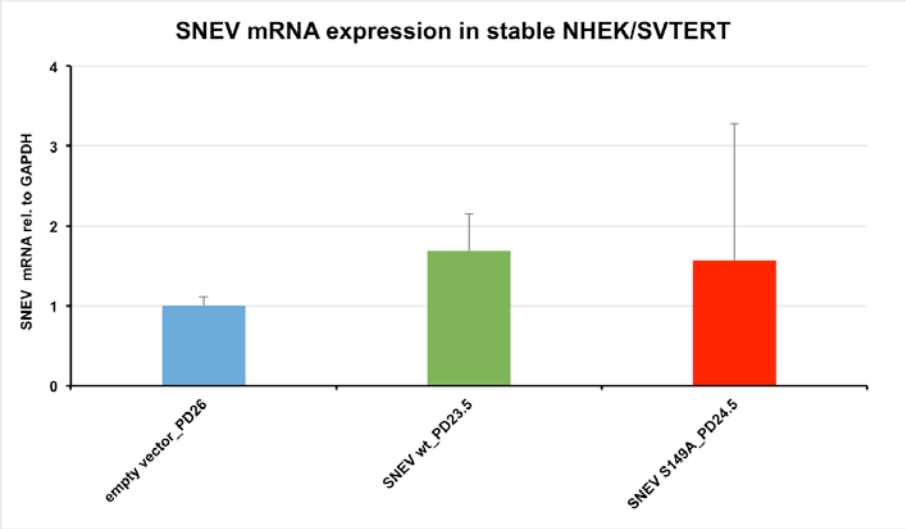

Figure 15: Conformation of successful *SNEV* overexpression in keratinocytes. Respective empty vector, *SNEV* wt and *SNEV*$^{(S149A)}$ mRNA expression levels in normal human keratinocytes.

4.2.2 *SNEV* overexpression modulates keratinocyte growth potential

To study a possible effect of *SNEV* on keratinocyte proliferation capacity, we performed a proliferation assay observing the cells for 10 days. We saw an induction of the proliferative capacity in *SNEV* wt at early time points (Fig.1&A). After six days in culture, the transduced NHEK/SVTERT started to develop vacuoles and rounded up, indicating that they are dying because they grew too dense (Fig. 16B). Consequently, after day 6 no reasonable determination of the cell number could be accomplished. The experiment needs to be repeated over a shorter timeframe, with shorter observation intervals. This could not be realized in this thesis due to a lack of time.

A

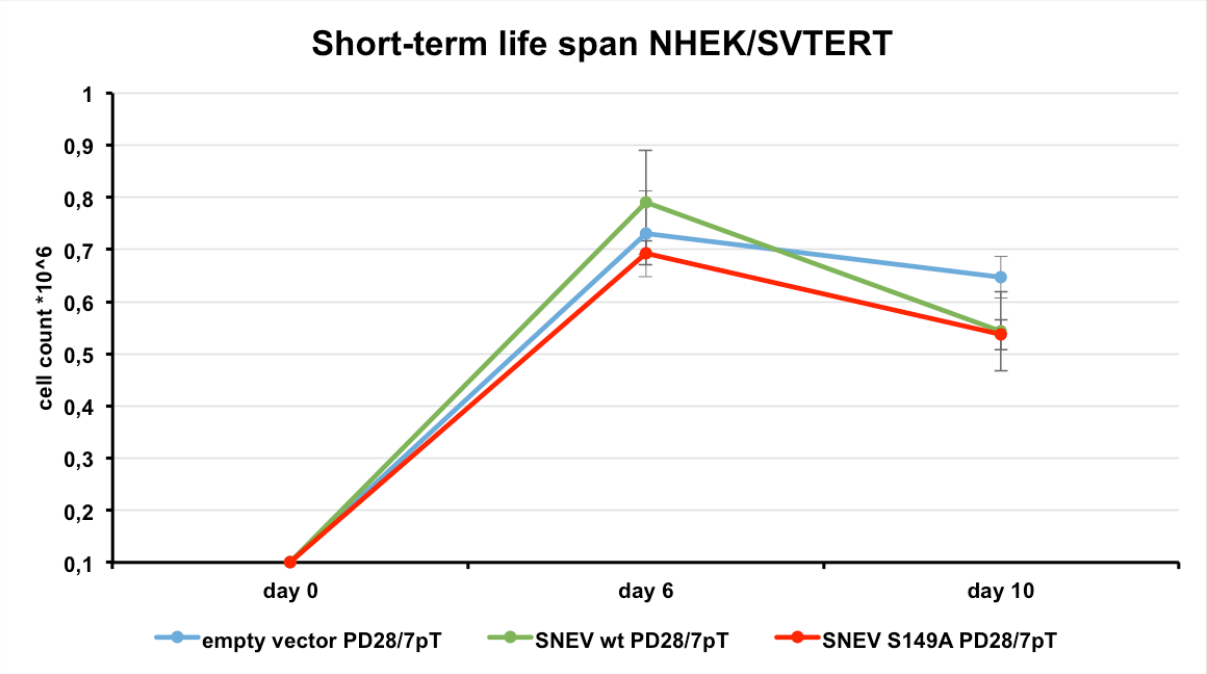

B

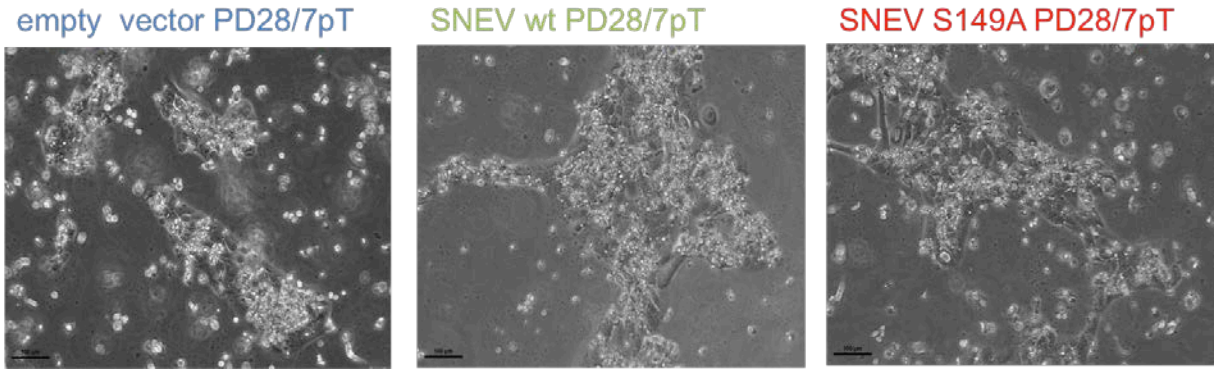

Figure 16: Effect of *SNEV* overexpression on human epidermal keratinocytes. (A) Proliferation assay over 10 days. Samples were analysed in triplicates. (B) Light microscopy pictures at day 10 of the proliferation assay. Scale bars 100 µm.

4.2.3 Effect of *SNEV* on keratinocyte migration

As the epidermis, the outermost layer of the skin is made of keratinocytes they are the first cells getting in contact with any kind of harmful substances but also mechanical damage. Therefore, we performed a scratch assay with a monolayer culture of the recombinant NHEK/SVTERT cell lines to determine the consequence of wounding on those cells and if *SNEV* affects the wound healing process.

In this scratch assays we did not observe significant differences between empty vector, *SNEV* wt and *SNEV*$^{(S149A)}$. Wild type *SNEV* overexpressing cells closed the wounded area only slightly faster than empty vector control cells (Fig. 17B). Interestingly, *SNEV*$^{(S149A)}$ displayed the quickest cell migration into the scratched area with a “wound closure” of 37 % after 9 hours.

A

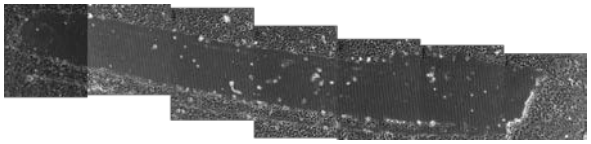

B

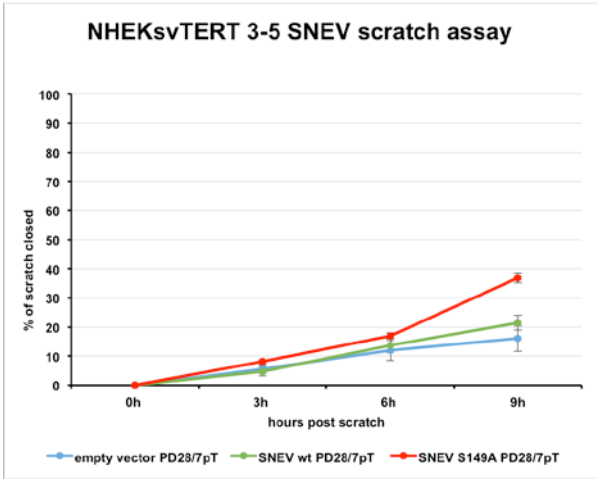

Figure 17: Effect of *SNEV* on keratinocyte migration into wounded area. (A) Wound healing assay of stable recombinant normal human epidermal keratinocyte cell lines.

5 Discussion

SNEV is a ubiquitously expressed, essential, multi-talented protein interacting with a plethora of proteins involved in cellular pathways like DNA repair, mRNA splicing and life span regulation. We established stable *SNEV* overexpressing fibroblast and keratinocyte cell lines to investigate its effects. It is not possible to complete the picture by showing the effect of *SNEV* knockdown, since *SNEV* is a highly stable protein and knockdown is technically difficult to achieve. Additionally, it is an essential protein, which means that as soon as a substantial knockdown is achieved, cells undergo apoptosis.

5.1 Effects of *SNEV* overexpression on human dermal fibroblasts

After we stably overexpressed *SNEV* in human dermal fibroblasts, various experiments were conducted to determine the influence of this protein on cellular growth, life span, functionality and differentiation status. Proliferation assays, qPCR, scratch assays, collagen contraction assays as well as staining for SA-β-gal expression levels gave us some indication of *SNEV* and the way it might function.

Concerning the role of *SNEV* in growth and senescence, we could not observe such a clear effect in counteracting aging as it was shown in human endothelial cells, by extending their cellular life span(Voglauer et al. 2006). *SNEV* overexpressing human dermal fibroblasts show a reduced growth potential, observed during long-term cultivation and short-term proliferation assays. A possible explanation is that cells with elevated *SNEV* levels seem to react more sensitive to DNA damage. This mirrors the fact that *SNEV* causes higher percentage of SA-β-gal positive cells. After chronic stress treatment, *SNEV* overexpressing fibroblasts show slightly less SA-β-gal expression. This emphasizes the theory that wild type *SNEV* overexpression in human dermal fibroblasts reduces growth but at the same time the cells are more capable to handle extrinsic stress.

Papillary to reticular transition is one of the most striking features on cellular level observed during aging. Reticular fibroblasts are described as cells showing a stellate morphology(Mine et al. 2008), reminiscent of senescent cells. In contrast, characteristic of papillary fibroblasts is a spindle-shaped morphology(Mine et al. 2008), which exactly could be observed after wild type *SNEV* overexpression. Even after prolonged culture of up to five months this phenotype didn't change a lot indicating that *SNEV* might slow down the transition from papillary into reticular fibroblasts and counteract aging. We could verify this hypothesis by light as well as fluorescence microscopy, analysing parameters perfectly reflecting the cellular shape. As someone might argue cellular morphology is difficult to quantify, we confirmed our findings by qPCR against established papillary and reticular marker genes. NTN1 and PDPN served as papillary marker genes and were higher expressed in *SNEV* overexpressing fibroblasts compared to empty vector control fibroblasts. For PPP1R14A and TGM-2, it was exactly the other way around. In the human dermis two subpopulations of fibroblasts reside building up the papillary and reticular dermis. Therefore, in a cell culture we have a mixture of papillary and reticular fibroblasts. The ratio between the two phenotypes is shifted during time of culture, in favour of the reticular subpopulation. *SNEV* changes this proportion, either by decelerating the differentiation of papillary to reticular fibroblasts, or by promoting the expression of papillary marker genes. Future investigation is necessary to determine the exact mechanism. Fibroblasts transduced with phosphorylation incompetent $SNEV^{(S149A)}$ behaved similar like empty vector control cells, even more clear in favour of the reticular phenotype indicating that the phosphorylation of *SNEV* is necessary for its effect on fibroblast morphology.

Another striking point is the strong influence of *SNEV* on wound healing. It enhances wound healing by multiple pathways. Scratch assays showed that keratinocytes cultivated with conditioned medium from wild type *SNEV* overexpressing fibroblasts migrate faster into the wounded area compared to cells cultivated with medium from fibroblasts transduced with empty vector. *SNEV* overexpressing fibroblasts may secret factors into the media that promote keratinocyte migration into the wounded area. At this time, these factors and their respective signalling pathways are still unknown. Interestingly, phosphorylation of *SNEV* seems to be partly dispensable as keratinocytes cultivated with media from fibroblasts transduced with phosphorylation mutated $SNEV^{(S149A)}$ still display faster wound closure as those cultivated with media from empty vector control cells. Another fact, supporting the

theory that *SNEV* not only indirectly but also directly influences wound healing in a positive way, is revealed by the verification that fibroblasts overexpressing the protein exhibit a higher content of α-smooth muscle actin. α-SMA is considered as a marker gene for myofibroblasts. The role of these cells in tissue repair is their ability of wound contraction and the synthesis of ECM, important for maturation and remodelling of granulation tissue(Darby et al. 2014). To investigate a role of *SNEV* in wound healing by an independent method, collagen contraction assays were performed. The assay allows you to analyse cell contractility and their mechanical force. In our experiments, we found no significant difference between *SNEV* overexpressing fibroblasts and empty vector control cells, regarding their contraction ability. No consistent results were obtained comparing these two recombinant cell lines with each other, indicating high technical variability of the assay. Nevertheless, phosphorylation seems to be essential for fibroblast contractility, as *SNEV*$^{(S149A)}$ showed a decreased potential to contract the gel. Further investigation and optimization of the collagen contraction assay are necessary to fully understand how *SNEV* influences the contraction ability of fibroblasts and therefore influences wound contraction and wound healing.

5.2 Effects of *SNEV* overexpression on human epidermal keratinocytes

We generated a stable *SNEV* overexpressing keratinocyte cell line. Proliferation and scratch assays were conducted to determine the role of *SNEV* in the function of human epidermal keratinocytes.

To investigate the effect of *SNEV* in cell growth we conducted a proliferation assay over 10 days. We couldn't show any significant difference between the three recombinant cell lines expressing either empty vector, wild type *SNEV* or the phosphorylation-mutated form $SNEV^{(S149A)}$. The keratinocytes started to die after 6 days in culture because they grew too dense. The proliferation assay needs to be repeated over 6 days with a shorter time interval to determine the exact cell number every day. Due to a lack of time this experiment couldn't be done during this thesis.

It emerged quite difficult to conduct experiments with our recombinant NHEK cell lines, as they are very susceptible to enter cell death when growing too dense. The scratch assay showed us that there is no significant difference in the potential of wound healing between *SNEV* wt and empty vector. Keratinocytes transduced with phosphorylation incompetent $SNEV^{(S149A)}$ displayed the fastest wound closure indicating that phosphorylation is dispensable for this process.

6 Conclusion

With this work we could gain further insights into the complex human protein *SNEV* and its ability to influence diverse molecular mechanisms. Especially its capability to influence human dermal fibroblast functions and characteristics could be nicely shown in this thesis. Further research is necessary to investigate how *SNEV* is exactly involved in these pathways. Also the overexpression of *SNEV* in other donor cell lines requires further investigation, as its effect seems to depend highly on the cell line that is transfected.

SNEV is a fascinating, multi-talented protein with a lot of features still waiting to be discovered.

7 References

Álvarez-Quilón A, Serrano-Benítez A, Lieberman JA, Quintero C, Sánchez-Gutiérrez D, Escudero LM, Cortés-Ledesma F. 2014. ATM specifically mediates repair of double-strand breaks with blocked DNA ends. Nature communications 5:3347.

Anatomy and Physiology. 1362.

Andreadis ST, Hamoen KE, Yarmush ML, Morgan JR. 2001. Keratinocyte growth factor induces hyperproliferation and delays differentiation in a skin equivalent model system. The FASEB journal : official publication of the Federation of American Societies for Experimental Biology 15:898–906.

Ashcroft GS, Horan MA, Ferguson MW. 1997. Aging is associated with reduced deposition of specific extracellular matrix components, an upregulation of angiogenesis, and an altered inflammatory response in a murine incisional wound healing model. The Journal of investigative dermatology 108(4):430–7.

Azzarone B, Macieira-Coelho A. 1982. Heterogeneity of the kinetics of proliferation within human skin fibroblastic cell populations. Journal of cell science 57:177–87.

Bakkenist CJ, Kastan MB. 2003. DNA damage activates ATM through intermolecular autophosphorylation and dimer dissociation. Nature 421(6922):499–506.

Barzilai N, Huffman DM, Muzumdar RH, Bartke A. 2012a. The critical role of metabolic pathways in aging. Diabetes 61(6):1315–1322.

Barzilai N, Huffman DM, Muzumdar RH, Bartke A. 2012b. The Critical Role of Metabolic Pathways in Aging. Diabetes 61(6):1315–1322.

Berkovich E, Monnat RJ, Kastan MB. 2007. Roles of ATM and NBS1 in chromatin structure modulation and DNA double-strand break repair. Nature cell biology 9(6):683–90.

Breuhahn K, Mann A, Müller G, Wilhelmi A, Schirmacher P, Enk A, Blessing M. 2000. Epidermal overexpression of granulocyte-macrophage colony-stimulating factor induces both keratinocyte proliferation and apoptosis. Cell growth & differentiation : the molecular biology journal of the American Association for Cancer Research 11(2):111–121.

Bruce SA, Deamond SF. 1991. Longitudinal study of in vivo wound repair and in vitro cellular senescence of dermal fibroblasts. Experimental gerontology 26(1):17–27.

Campisi J. 2013. Aging, cellular senescence, and cancer. Annual review of physiology 75:685–705.

Chan S-P, Cheng S-C. 2005. The Prp19-associated Complex Is Required for Specifying Interactions of U5 and U6 with Pre-mRNA during Spliceosome Activation. Journal of Biological Chemistry 280(35):31190–31199.

Chan SP, Kao DI, Tsai WY, Cheng SC. 2003. The prp19p-associated complex in spliceosome activation. Science 302(5643):279–82.

Chanarat S, Sträßer K. 2013. Splicing and beyond: The many faces of the Prp19 complex. Biochimica et Biophysica Acta (BBA) - Molecular Cell Research 1833(10):2126–34.

Chanarat S, Seizl M, Strässer K. 2011. The Prp19 complex is a novel transcription elongation factor required for TREX occupancy at transcribed genes. Genes Dev 25:1147–1158.

Chen HR, Jan SP, Tsao TY, Sheu YJ, Banroques J, Cheng SC. 1998. Snt309p, a component of the Prp19p-associated complex that interacts with Prp19p and associates with the spliceosome simultaneously with or immediately after dissociation of U4 in the same manner as Prp19p. Molecular and cellular biology 18(4):2196–204.

Collado M, Blasco MA, Serrano M. 2007. Cellular Senescence in Cancer and Aging. Cell 130(2):223–233.

Coppé J-P, Kauser K, Campisi J, Beauséjour CM. 2006. Secretion of vascular endothelial growth factor by primary human fibroblasts at senescence. The Journal of biological chemistry 281(40):29568–74.

Coppé J-P, Desprez P-Y, Krtolica A, Campisi J. 2010. The senescence-associated secretory phenotype: the dark side of tumor suppression. Annual review of pathology 5:99–118.

Darby IA, Laverdet B, Bonté F, Desmoulière A. 2014. Fibroblasts and myofibroblasts in wound healing. Clinical, Cosmetic and Investigational Dermatology 7:301–311.

Davalos AR, Coppe JP, Campisi J, Desprez PY. 2010. Senescent cells as a source of inflammatory factors for tumor progression. Cancer and Metastasis Reviews 29(2):273–283.

Deckert J, Hartmuth K, Boehringer D, Behzadnia N, Will CL, Kastner B, Stark H, Urlaub H, Luhrmann R. 2006. Protein Composition and Electron Microscopy Structure of Affinity-Purified Human Spliceosomal B Complexes Isolated under Physiological Conditions. Molecular and Cellular Biology 26(14):5528–5543.

Dellago H, Oscher M, Ajuh P, Ryder U, Kaisermayer C, Grillari-Voglauer R, Fortschegger K, Gross S, Gstraunthaler A, Borth N, et al. 2011. Exo70, a subunit of the exocyst complex, interacts with SNEV hPrp19/hPso4 and is involved in pre-mRNA splicing. Biochem. J 438:81–91.

Dellago H, Khan A, Nussbacher M, Gstraunthaler A, Lämmermann I, Schosserer M, Mück C, Anrather D, Scheffold A, Ammerer G, et al. 2012. ATM-dependent phosphorylation of SNEVhPrp19/hPso4 is involved in extending cellular life span and suppression of apoptosis. Aging (Albany NY) 4(4):290–304.

Ding D, Zhang Y, Yu H, Guo Y, Jiang L, He X, Ma W, Zheng W. 2012. Genetic variation of XPA gene and risk of cancer: A systematic review and pooled analysis. International Journal of Cancer 131(2):488–496.

Domínguez-Sánchez MS, Barroso S, Gómez-González B, Luna R, Aguilera A. 2011. Genome Instability and Transcription Elongation Impairment in Human Cells Depleted of THO/TREX (CE Pearson, Ed). PLoS Genetics 7(12):e1002386.

Donaldson DJ, Mahan JT, Smith GN. 1987. Newt epidermal cell migration in vitro and in vivo appears to involve Arg-Gly-Asp-Ser receptors. Journal of cell science 87 (Pt 4):525–34.

Driskell RR, Lichtenberger BM, Hoste E, Kretzschmar K, Simons BD, Charalambous M, Ferron SR, Herault Y, Pavlovic G, Ferguson-Smith AC, et al. 2013. Distinct fibroblast lineages determine dermal architecture in skin development and repair. Nature 504(7479):277–81.

Eisenberg E, Levanon EY. 2013. Human housekeeping genes, revisited. Trends in Genetics 29(10):569–574.

Elias PM, Goerke J, Friend DS. 1977. Mammalian Epidermal Barrier Layer Lipids: Composition and Influence on Structure. Journal of Investigative Dermatology 69(6):535–546.

Epstein FH, Singer AJ, Clark RAF. 1999. Cutaneous Wound Healing. New England Journal of Medicine 341(10):738–746.

Fang JY, Wang PW, Huang CH, Chen MH, Wu YR, Pan TL. 2016. Skin aging caused by intrinsic or extrinsic processes characterized with functional proteomics. Proteomics 16(20):2718–2731.

Fortschegger K, Wagner B, Voglauer R, Katinger H, Sibilia M, Grillari J. 2007. Early embryonic lethality of mice lacking the essential protein SNEV. Mol Cell Biol 27(8):3123–3130.

Fraga MF, Esteller M. 2007. Epigenetics and aging: the targets and the marks. Trends in Genetics 23(8):413–418.

Franceschi C. 2007. Inflammaging as a Major Characteristic of Old People: Can It Be Prevented or Cured? Nutrition Reviews 65(SUPPL.3).

Freund A, Orjalo A V., Desprez PY, Campisi J. 2010. Inflammatory networks during cellular senescence: causes and consequences. Trends in Molecular Medicine 16(5):238–246.

Garinis GA, van der Horst GTJ, Vijg J, Hoeijmakers JHJ. 2008. DNA damage and ageing: new-age ideas for an age-old problem. Nature cell biology 10(11):1241–7.

González-Barrera S, Prado F, Verhage R, Brouwer J, Aguilera A. 2002. Defective nucleotide excision repair in yeast hpr1 and tho2 mutants. Nucleic acids research 30(10):2193–201.

Gosain A, DiPietro LA. 2004. Aging and Wound Healing. World Journal of Surgery 28(3):321–326.

Gotzmann J, Gerner C, Meissner M, Holzmann K, Grimm R, Mikulits W, Sauermann G. 2000. hNMP 200: A novel human common nuclear matrix protein combining structural and regulatory functions. Exp Cell Res 261:166–79.

Green DR, Galluzzi L, Kroemer G. 2011. Mitochondria and the autophagy-inflammation-cell death axis in organismal aging. Science (New York, N.Y.) 333(6046):1109–12.

Grey M, Düsterhöft A, Henriques JA, Brendel M. 1996. Allelism of PSO4 and PRP19 links pre-mRNA processing with recombination and error-prone DNA repair in Saccharomyces cerevisiae. Nucleic Acids Res 24:4009–4014.

Grillari J, Hohenwarter O, Grabherr RM, Katinger H. 2000. Subtractive Hybridization of mRNA from early passage and senescent endothelial cells. Experimental Gerontology 35(2):187–197.

Grillari J, Ajuh P, Stadler G, Löscher M, Voglauer R, Ernst W, Chusainow J, Eisenhaber F, Pokar M, Fortschegger K, et al. 2005. SNEV is an evolutionarily conserved splicing factor whose oligomerization is necessary for spliceosome assembly. Nucleic acids research 33(21):6868–83.

Grillari J, Löscher M, Denegri M, Lee K, Fortschegger K, Eisenhaber F, Ajuh P, Lamond AI, Katinger H, Grillari-Voglauer R. 2009. Blom7alpha is a novel heterogeneous nuclear ribonucleoprotein K homology domain protein involved in pre-mRNA splicing that interacts with SNEVPrp19-Pso4. J Biol Chem 284:29193–29204.

Grote M, Wolf E, Will CL, Lemm I, Agafonov DE, Schomburg A, Fischle W, Urlaub H, Lührmann R. 2010. Molecular architecture of the human Prp19/CDC5L complex. Mol Cell Biol 30:2105–2119.

Grove GL, Kligman AM. 1983. Age-associated changes in human epidermal cell renewal. Journal of gerontology 38(2):137–42.

Gunin AG, Kornilova NK, Vasilieva O V., Petrov V V. 2011. Age-related changes in proliferation, the numbers of mast cells, eosinophils, and cd45-positive cells in human dermis. Journals of Gerontology - Series A Biological Sciences and Medical Sciences 66 A(4):385–392.

Gunin AG, Petrov V V., Golubtzova NN, Vasilieva O V., Kornilova NK. 2014. Age-related changes in angiogenesis in human dermis. Experimental Gerontology 55:143–151.

Harper RA, Grove G. 1979. Human skin fibroblasts derived from papillary and reticular dermis: differences in growth potential in vitro. Science (New York, N.Y.) 204(4392):526–7.

Harrison DE, Strong R, Sharp ZD, Nelson JF, Astle CM, Flurkey K, Nadon NL, Wilkinson JE, Frenkel K, Carter CS, et al. 2009. Rapamycin fed late in life extends lifespan in genetically heterogeneous mice. Nature 460(7253):392–5.

Hatakeyama S, Nakayama KI. 2003. U-box proteins as a new family of ubiquitin ligases. Biochemical and biophysical research communications 302(4):635–45.

HAYFLICK L, MOORHEAD PS. 1961. The serial cultivation of human diploid cell strains. Experimental cell research 25:585–621.

Hekimi S, Lapointe J, Wen Y. 2011. Taking a 'good' look at free radicals in the aging process. Trends in Cell Biology 21(10):569–576.

Hinz B, Gabbiani G. 2003. Cell-matrix and cell-cell contacts of myofibroblasts: role in connective tissue remodeling. Thrombosis and Haemostasis 90(6):993–1002.

Hoeijmakers JHJ. 2009. DNA Damage, Aging, and Cancer. New England Journal of Medicine 361(15):1475–1485.

Howard SM, Yanez DA, Stark JM. 2015. DNA Damage Response Factors from Diverse Pathways, Including DNA Crosslink Repair, Mediate Alternative End Joining (N Maizels, Ed). PLOS Genetics 11(1):e1004943.

Janson D, Saintigny G, Mahé C, Ghalbzouri A El. 2013. Papillary fibroblasts differentiate into reticular fibroblasts after prolonged in vitro culture. Experimental Dermatology 22(1):48–53.

Janson DG, Saintigny G, van Adrichem A, Mahé C, El Ghalbzouri A. 2012. Different Gene Expression Patterns in Human Papillary and Reticular Fibroblasts. Journal of Investigative Dermatology 132(11):2565–2572.

Jaskelioff M, Muller FL, Paik J-H, Thomas E, Jiang S, Adams AC, Sahin E, Kost-Alimova M, Protopopov A, Cadiñanos J, et al. 2011. Telomerase reactivation reverses tissue degeneration in aged telomerase-deficient mice. Nature 469(7328):102–6.

Jones P a, Baylin SB. 2002. The fundamental role of epigenetic events in cancer. Nature reviews. Genetics 3(6):415–28.

Kakarougkas A, Jeggo PA. 2014. DNA DSB repair pathway choice: an orchestrated handover mechanism. The British Journal of Radiology 87(1035):20130685.

Kastan MB, Lim D. 2000. The many substrates and functions of ATM. Nature Reviews Molecular Cell Biology 1(3):179–186.

Kaufmann WK. 2010. The human intra-S checkpoint response to UVC-induced DNA damage. Carcinogenesis 31(5):751–765.

Koga H, Kaushik S, Cuervo a M. 2012. Protein Homeostasis and Aging: the importance of exquisite quality control. Ageing Res. Rev. 10(2):205–215.

Vander Kooi CW, Ohi MD, Rosenberg JA, Oldham ML, Newcomer ME, Gould KL, Chazin WJ. 2006. The Prp19 U-box crystal structure suggests a common dimeric architecture for a class of oligomeric E3 ubiquitin ligases. Biochemistry 45:121–130.

Vander Kooi CW, Ren L, Xu P, Ohi MD, Gould KL, Chazin WJ. 2010. The Prp19 WD40 domain contains a conserved protein interaction region essential for its function. Structure 18:584–593.

Krtolica A, Larocque N, Genbacev O, Ilic D, Coppe JP, Patil CK, Zdravkovic T, McMaster M, Campisi J, Fisher SJ. 2011. GRO?? regulates human embryonic stem cell self-renewal or adoption of a neuronal fate. Differentiation 81(4):222–232.

Kuraoka I, Ito S, Wada T, Hayashida M, Lee L, Saijo M, Nakatsu Y, Matsumoto M, Matsunaga T, Handa H, et al. 2008. Isolation of XAB2 complex involved in pre-mRNA splicing, transcription, and transcription-coupled repair. J Biol Chem 283:940–950.

Laberge RM, Awad P, Campisi J, Desprez PY. 2012. Epithelial-mesenchymal transition induced by senescent fibroblasts. Cancer Microenvironment 5(1):39–44.

Lavker RM, Zheng PS, Dong G. 1987. Aged skin: a study by light, transmission electron, and scanning electron microscopy. The Journal of investigative dermatology 88(3 Suppl):44s–51s.

Lee JW, Harrigan J, Opresko PL, Bohr VA. 2005a. Pathways and functions of the Werner syndrome protein. Mechanisms of Ageing and Development 126(1):79–86.

Lee JW, Harrigan J, Opresko PL, Bohr VA. 2005b. Pathways and functions of the Werner syndrome protein. Mechanisms of Ageing and Development 126(1):79–86.

Lim DS, Kim ST, Xu B, Maser RS, Lin J, Petrini JH, Kastan MB. 2000. ATM phosphorylates p95/nbs1 in an S-phase checkpoint pathway. Nature 404(6778):613–7.

Longaker MT, Adzick NS. 1991. The biology of fetal wound healing: a review. Plastic and reconstructive surgery 87(4):788–98.

López-Otín C, Blasco MA, Partridge L, Serrano M, Kroemer G. 2013. The hallmarks of aging. Cell 153(6):1194–217.

Löscher M, Fortschegger K, Ritter G, Wostry M, Voglauer R, Schmid JA, Watters S, Rivett AJ, Ajuh P, Lamond AI, et al. 2005. Interaction of U-box E3 ligase SNEV with PSMB4, the beta7 subunit of the 20 S proteasome. The Biochemical journal 388(Pt 2):593–603.

Lu X, Legerski RJ. 2007. The Prp19/Pso4 core complex undergoes ubiquitylation and structural alterations in response to DNA damage. Biochem Biophys Res Commun 354:968–974.

Macieira-Coelho A. 1997. Genetics of aging. Comptes rendus des seances de la Societe de biologie et de ses filiales 191(October):545–551.

Mahajan K. 2015. hPso4/hPrp19: a critical component of DNA repair and DNA damage checkpoint complexes. Oncogene.

Mahajan KN, Mitchell BS. 2003. Role of human Pso4 in mammalian DNA repair and association with terminal deoxynucleotidyl transferase. Proc Natl Acad Sci U S A 100(19):10746–51.

Makarov EM, Makarova O V, Urlaub H, Gentzel M, Will CL, Wilm M, Lührmann R. 2002. Small nuclear ribonucleoprotein remodeling during catalytic activation of the spliceosome. Science (New York, N.Y.) 298(5601):2205–8.

Makarova O V, Makarov EM, Urlaub H, Will CL, Gentzel M, Wilm M, Lührmann R. 2004. A subset of human 35S U5 proteins, including Prp19, function prior to catalytic step 1 of splicing. The EMBO journal 23(12):2381–91.

Mao F, Leung W-Y, Xin X. 2007. Characterization of EvaGreen and the implication of its physicochemical properties for qPCR applications. BMC Biotechnology 7(1):76.

Maréchal A, Li J-M, Ji XY, Wu C-S, Yazinski SA, Nguyen HD, Liu S, Jiménez AE, Jin J, Zou L. 2014. PRP19 transforms into a sensor of RPA-ssDNA after DNA damage and drives ATR activation via a ubiquitin-mediated circuitry. Molecular cell 53(2):235–46.

Martins SB, Rino J, Carvalho T, Carvalho C, Yoshida M, Klose JM, de Almeida SF, Carmo-Fonseca M. 2011. Spliceosome assembly is coupled to RNA polymerase II dynamics at the 3' end of human genes. Nature structural & molecular biology 18(10):1115–23.

Mine S, Fortunel NO, Pageon H, Asselineau D. 2008. Aging alters functionally human dermal papillary fibroblasts but not reticular fibroblasts: a new view of skin morphogenesis and aging. PloS one 3(12):e4066.

Molofsky A V., Slutsky SG, Joseph NM, He S, Pardal R, Krishnamurthy J, Sharpless NE, Morrison SJ. 2006. Increasing p16INK4a expression decreases forebrain progenitors and neurogenesis during ageing. Nature 443(7110):448–452.

Montagna W, Carlisle K. 1979. Structural changes in aging human skin. The Journal of Investigative Dermatology 73(1):47–53.

Morrison TB, Weis JJ, Wittwer CT. 1998. Quantification of low-copy transcripts by continuous SYBR Green I monitoring during amplification. BioTechniques 24(6):954–8, 960, 962.

Motoyama N, Naka K. 2004. DNA damage tumor suppressor genes and genomic instability. Current opinion in genetics & development 14(1):11–6.

Nakatsu Y, Asahina H, Citterio E, Rademakers S, Vermeulen W, Kamiuchi S, Yeo J-P, Khaw M-C, Saijo M, Kodo N, et al. 2000. XAB2, a Novel Tetratricopeptide Repeat Protein Involved in Transcription-coupled DNA Repair and Transcription. Journal of Biological Chemistry 275(45):34931–34937.

Nelson G, Wordsworth J, Wang C, Jurk D, Lawless C, Martin-Ruiz C, von Zglinicki T. 2012. A senescent cell bystander effect: senescence-induced senescence. Aging Cell 11(2):345–349.

Du Noüy PL. 1916. CICATRIZATION OF WOUNDS : III. THE RELATION BETWEEN THE AGE OF THE PATIENT, THE AREA OF THE WOUND, AND THE INDEX OF CICATRIZATION. The Journal of experimental medicine 24(5):461–70.

Ohi MD, Gould KL. 2002. Characterization of interactions among the Cef1p-Prp19p-associated splicing complex. RNA (New York, N.Y.) 8(6):798–815.

Ohi MD, Vander Kooi CW, Rosenberg JA, Chazin WJ, Gould KL. 2003. Structural insights into the U-box, a domain associated with multi-ubiquitination. Nature structural biology 10(4):250–5.

Ohi MD, Vander Kooi CW, Rosenberg JA, Ren L, Hirsch JP, Chazin WJ, Walz T, Gould KL. 2005. Structural and functional analysis of essential pre-mRNA splicing factor Prp19p. Mol Cell Biol 25:451–460.

Paull TT. 2015. Mechanisms of ATM Activation. Annual Review of Biochemistry 84(1):711–738.

Payne BAI, Chinnery PF. 2015. Mitochondrial dysfunction in aging: Much progress but many unresolved questions. Biochimica et Biophysica Acta (BBA) - Bioenergetics 1847(11):1347–1353.

Pickart CM. 2001. Mechanisms Underlying Ubiquitination. Annual Review of Biochemistry 70(1):503–533.

Pittman J. 2007. Effect of Aging on Wound Healing. Journal of Wound, Ostomy and Continence Nursing 34(4):412–417.

Powers ET, Morimoto RI, Dillin A, Kelly JW, Balch WE. 2009. Biological and chemical approaches to diseases of proteostasis deficiency. Annual review of biochemistry 78(August):959–991.

Raeymaekers L. 2000. Basic principles of quantitative PCR. Molecular biotechnology 15(2):115–122.

Ririe KM, Rasmussen RP, Wittwer CT. 1997. Product Differentiation by Analysis of DNA Melting Curves during the Polymerase Chain Reaction. Analytical Biochemistry 245(2):154–160.

Rittie L, Fisher GJ. 2015. Natural and Sun-Induced Aging of Human Skin. Cold Spring Harbor Perspectives in Medicine 5(1):a015370–a015370.

Rodier F, Campisi J. 2011. Four faces of cellular senescence. Journal of Cell Biology 192(4):547–556.

Rossi DJ, Jamieson CHM, Weissman IL. 2008. Stems Cells and the Pathways to Aging and Cancer. Cell 132(4):681–696.

Rubin JS, Bottaro DP, Chedid M, Miki T, Ron D, Cheon G, Taylor WG, Fortney E, Sakata H, Finch PW, et al. 1995. Keratinocyte growth factor. Cell Biology International 19(5):399–411.

Salminen A, Kaarniranta K, Kauppinen A. 2012. Inflammaging: disturbed interplay between autophagy and inflammasomes. Aging 4(3):166–175.

SANDBLOM P. Determination of the tensile strength of the healing wound as a clinical test. Journal international de chirurgie 13(4):Extra pages, 1–4.

Shackelford RE, Innes CL, Sieber SO, Heinloth AN, Leadon SA, Paules RS. 2001. The Ataxia telangiectasia Gene Product Is Required for Oxidative Stress-induced G1 and G2Checkpoint Function in Human Fibroblasts. Journal of Biological Chemistry 276(24):21951–21959.

Shaw AC, Joshi S, Greenwood H, Panda A, Lord JM. 2010. Aging of the innate immune system. Current Opinion in Immunology 22(4):507–513.

Shay JW, Zou Y, Hiyama E, Wright WE. 2001. Telomerase and cancer. Human molecular genetics 10(7):677–85.

Da Silva K V, de Morais Júnior MA, Henriques JA. 1995. The PSO4 gene of S. cerevisiae is important for sporulation and the meiotic DNA repair of photoactivated psoralen lesions. Curr Genet 27:207–212.

Skin Structure infographic - LifeMap Discovery.

Song EJ, Werner SL, Neubauer J, Stegmeier F, Aspden J, Rio D, Harper JW, Elledge SJ, Kirschner MW, Rape M. 2010. The Prp19 complex and the Usp4Sart3 deubiquitinating enzyme control reversible ubiquitination at the spliceosome. Genes & development 24(13):1434–47.

Sorrell JM, Caplan AI. 2004. Fibroblast heterogeneity: more than skin deep. Journal of cell science 117(Pt 5):667–75.

Sorrell JM, Carrino DA, Baber MA, Caplan AI. 1999. Versican in human fetal skin development. Anatomy and Embryology 199(1):45–56.

Sorrell JM, Baber MA, Caplan AI. 2004. Site-matched papillary and reticular human dermal fibroblasts differ in their release of specific growth factors/cytokines and in their interaction with keratinocytes. Journal of Cellular Physiology 200(1):134–145.

Tarn WY, Hsu CH, Huang KT, Chen HR, Kao HY, Lee KR, Cheng SC. 1994. Functional association of essential splicing factor(s) with PRP19 in a protein complex. EMBO J 13:2421–2431.

Tornaletti S. 2009. DNA repair in mammalian cells: Transcription-coupled DNA repair: directing your effort where it's most needed. Cellular and molecular life sciences : CMLS 66(6):1010–20.

Ulfig N. 2005. Kurzlehrbuch Histologie

Voglauer R, Chang MWF, Dampier B, Wieser M, Baumann K, Sterovsky T, Schreiber M, Katinger H, Grillari J. 2006. SNEV overexpression extends the life span of human endothelial cells. Experimental Cell Research 312(6):746–759.

Wan L, Huang J. 2014. The PSO4 protein complex associates with replication protein A (RPA) and modulates the activation of ataxia telangiectasia-mutated and Rad3-related (ATR). The Journal of biological chemistry 289(10):6619–26.

Werner S, Smola H. 2001. Paracrine regulation of keratinocyte proliferation and differentiation. Trends in Cell Biology 11(4):143–146.

Will CL, Luhrmann R. 2011. Spliceosome Structure and Function. Cold Spring Harbor Perspectives in Biology 3(7):a003707–a003707.

Williams GC. 1957. Pleiotropy, Natural Selection, and the Evolution of Senescence. Evolution 11(4):398.

Woodley DT. 2017. Distinct Fibroblasts in the Papillary and Reticular Dermis. Dermatologic Clinics 35(1):95–100.

Woodley DT, Wysong A, DeClerck B, Chen M, Li W. 2015. Keratinocyte Migration and a Hypothetical New Role for Extracellular Heat Shock Protein 90 Alpha in Orchestrating Skin Wound Healing. Advances in wound care 4(4):203–212.

Worman HJ. 2012. Nuclear lamins and laminopathies. The Journal of pathology 226(2):316–25.

Xu B, O'Donnell AH, Kim S-T, Kastan MB. 2002. Phosphorylation of serine 1387 in Brca1 is specifically required for the Atm-mediated S-phase checkpoint after ionizing irradiation. Cancer research 62(16):4588–91.

Yang G, Rosen DG, Zhang Z, Bast RC, Mills GB, Colacino JA, Mercado-Uribe I, Liu J. 2006. The chemokine growth-regulated oncogene 1 (Gro-1) links RAS signaling to the senescence of stromal fibroblasts and ovarian tumorigenesis. Proceedings of the National Academy of Sciences 103(44):16472–7.

Yin J, Zhu JM, Shen XZ. 2012. New insights into pre-mRNA processing factor 19: A multi-faceted protein in humans. Biology of the Cell.

Zhang J, Dewar JM, Budzowska M, Motnenko A, Cohn MA, Walter JC. 2015. DNA interstrand cross-link repair requires replication-fork convergence. Nature structural & molecular biology 22(3):242–7.

Zhang N, Kaur R, Lu X, Shen X, Li L, Legerski RJ. 2005. The Pso4 mRNA splicing and DNA repair complex interacts with WRN for processing of DNA interstrand cross-links. J Biol Chem 280:40559–40567.

Zhang N, Kaur R, Akhter S, Legerski RJ. 2009. Cdc5L interacts with ATR and is required for the S-phase cell-cycle checkpoint. EMBO Rep 10:1029–1035.